

Compact Groups of Galaxies selected by stellar mass: The 2MASS Compact Group Catalogue

Eugenia Díaz-Giménez^{1,2,3}, Gary A. Mamon⁴, Marcela Pacheco¹,

Claudia Mendes de Oliveira³ & M. Victoria Alonso^{1,2}

¹ *Instituto de Astronomía Teórica y Experimental, IATE, CONICET, Argentina*

² *Observatorio Astronómico, Universidad Nacional de Córdoba, Laprida 854, X5000BGR, Córdoba, Argentina*

³ *Instituto de Astronomia, Geofísica e Ciências Atmosféricas, IAG, USP, Rua do Matão 1226, São Paulo, Brazil*

⁴ *Institut d'Astrophysique de Paris (UMR 7095: CNRS & UPMC), 98 bis Bd Arago, F-75014 Paris, France*

28 October 2021

ABSTRACT

We present a photometric catalogue of compact groups of galaxies ($p2MCGs$) automatically extracted from the 2MASS extended source catalogue. A total of 262 $p2MCGs$ are identified, following the criteria defined by Hickson (1982), of which 230 survive visual inspection (given occasional galaxy fragmentation and blends in the 2MASS parent catalogue). Only one quarter of these 230 groups were previously known compact groups (CGs). Among the 144 $p2MCGs$ that have all their galaxies with known redshifts, 85 (59%) have 4 or more accordant galaxies. This $v2MCG$ sample of velocity-filtered $p2MCGs$ constitutes the largest sample of CGs (with $N \geq 4$) catalogued to date, with both well-defined selection criteria and velocity filtering, and is the first CG sample selected by stellar mass. It is fairly complete up to $K_{\text{group}} \sim 9$ and radial velocity of $\sim 6000 \text{ km s}^{-1}$.

We compared the properties of the 78 $v2MCGs$ with median velocities greater than 3000 km s^{-1} with the properties of other CG samples, as well as those ($mvCGs$) extracted from the semi-analytical model (SAM) of Guo et al. (2011) run on the high-resolution Millennium-II simulation. This $mvCG$ sample is similar (i.e. with 2/3 of physically dense CGs) to those we had previously extracted on three other SAMs run on the Millennium simulation with 125 times worse spatial and mass resolutions. The space density of $v2MCGs$ within 6000 km s^{-1} is $8.0 \times 10^{-5} h^3 \text{ Mpc}^{-3}$, i.e. 4 times that of the Hickson sample (HCG) up to the same distance and with the same criteria used in this work, but still 40% less than that of $mvCGs$.

The $v2MCG$ constitutes the first group catalogue to show a statistically large first-second ranked galaxy magnitude difference (in units of the dispersion of the first-ranked absolute magnitudes) according to Tremaine-Richstone statistics, as expected if the first ranked group members tend to be the products of galaxy mergers, and as confirmed in the $mvCGs$. The $v2MCG$ is also the first observed sample to show that first-ranked galaxies tend to be centrally located, again consistent with the predictions obtained from $mvCGs$. We found no significant correlation of group apparent elongation and velocity dispersion in the quartets among the $v2MCGs$, and the velocity dispersions of apparently round quartets are not significantly larger than those of chain-like ones, in contrast to what has been previously reported in HCGs.

By virtue of its automatic selection with the popular Hickson criteria, its size, its selection on stellar mass, and its statistical signs of mergers and centrally located brightest galaxies, the $v2MCG$ catalogue appears to be the laboratory of choice to study physically dense groups of 4 or more galaxies of comparable luminosity.

Key words: catalogues — galaxies: clusters: general — galaxies: interactions

1 INTRODUCTION

Compact Groups (hereafter, CGs) of at least 4 galaxies of comparable luminosity are the densest galaxy associations

known at present. The compactness of these groups is so high that the typical projected separations between galaxies are of the order of their own diameters (Hickson et al. 1992; Focardi & Kelm 2002), hence their space densities can exceed those of the cores of rich clusters. The combination of their very high number densities and low velocity dispersion makes CGs the ideal site of galaxy mergers (Mamon 1992, see also Carnevali et al. 1981; Barnes 1985; Mamon 1987a; Bode et al. 1993).

Since the discovery of Stephan’s Quintet (Stephan 1877) and Seyfert’s Sextet (Seyfert 1948), several surveys of CGs have been undertaken: Rose (1977) and Hickson (1982) performed visual identifications of CGs on the POSS I photographic plates. Thereafter, the new catalogues of CGs used automatic searches: from the COSMOS/UKST Southern Galaxy Catalogue (Prandoni et al. 1994; Iovino 2002), the DPOSS catalogue (Iovino et al. 2003; de Carvalho et al. 2005), and the Sloan Digital Sky Survey (SDSS) photometric catalogue DR1 (Lee et al. 2004) and DR6 (McConnachie et al. 2009). All of the above studies used only 2-dimensional information of the galaxies (i.e., angular positions). Other CG catalogues were obtained by searches in redshift space, e.g.: Barton et al. (1996) from the the CfA2 catalogue, Allam & Tucker (2000) from the Las Campanas Redshift Survey, Focardi & Kelm (2002) from the UZC Galaxy Catalogue, and Deng et al. (2008) from the SDSS-DR6 spectroscopic catalogue.

Since the nearly full spectroscopic followup by Hickson et al. (1992) of the original Hickson Compact Groups (Hickson 1982, hereafter, HCGs), the velocity-filtered sample of 92 HCGs with at least 3 accordant-redshift members and 69 with at least 4 has been, by far, the most studied to date (e.g. Hickson et al. 1989 for optical photometry; Mendes de Oliveira & Hickson 1991 for galaxy morphologies; Moles et al. 1994, de la Rosa et al. 2007 and Tzanavaris et al. 2010 for star formation rates; Coziol et al. 1998 for nuclear activity; de la Rosa et al. 2001 and Torres-Flores et al. 2010 for galaxy scaling relations; Verdes-Montenegro et al. 2001 and Borthakur et al. 2010 for neutral gas content; Ponman et al. 1996 for hot gas content, etc.).

However, the visual inspection performed by Hickson (1982) led to a sample of CGs that is not reproducible, incomplete and not homogeneous (Hickson et al. 1989; Walke & Mamon 1989; Prandoni et al. 1994; Sulentic 1997; Díaz-Giménez & Mamon 2010). In particular, using the $z = 0$ outputs of semi-analytical models of galaxy formation run on the Millennium cosmological dark matter simulation (Springel et al. 2005), Díaz-Giménez & Mamon (2010) have shown that the HCG sample is typically less than 10% complete at the median distance of the sample.

The properties of CGs and their member galaxies must be studied using complete and well-defined observed samples. To achieve this goal, we present a new sample of automatically selected CGs extracted from the largest solid angle catalogue at present, the 2 Micron All Sky Survey. Using 2MASS has two strong advantages: 1) it provides us with a full-sky survey and 2) the K -band photometry is only weakly sensitive to both galactic extinction, internal extinction and recent star formation, and is thus a very good tracer of the stellar mass content of galaxies. For these reasons, it is ideal to build a CG sample from a wide K -band galaxy

survey such as 2MASS (which has the additional benefit of being all-sky) with (nearly) full redshift information available from other sources (Mamon 1994).

The layout of this paper is as follows. In Sect. 2, we describe the parent catalogue. In Sect. 3, we present the CG catalogue. We perform a cross-identification between the 2MASS-CGs and other samples of groups in Sect. 4. In Sect. 5, we present a sample of CG after applying a velocity filtering, while we present some general properties of the samples in Sect. 6, and summarise and discuss our results in Sect. 7.

Throughout this paper we use a Hubble constant $H_0 = 100 h \text{ km s}^{-1} \text{ Mpc}^{-1}$, and for all cosmology-dependent calculations, we assume a flat cosmological model with a non-vanishing cosmological constant: $\Omega_m = 0.25$ and $\Omega_\Lambda = 0.75$.

2 THE PARENT CATALOGUE: 2MASS XSC

The 2 Micron All Sky Survey (2MASS) (Skrutskie et al. 2006) has uniformly scanned the entire sky in three near-infrared bands to detect and characterise point sources brighter than about 1 mJy in each band, with S/N greater than 10. 2MASS used two highly-automated 1.3-m telescopes, one at Mt. Hopkins, AZ, and one at CTIO, Chile. Each telescope was equipped with a three-channel camera, each channel consisting of a NICMOS3 256×256 HgCdTe array, capable of imaging a $8'.5 \times 8'.5$ field at a pixel scale of $2''$ per pixel in the J (1.25 microns), H (1.65 microns), and K_s (2.17 microns) bands.

Our data set was selected from the publicly available full-sky extended source catalogue (XSC; Jarrett et al. 2000)¹, which contains over 1.6 million extended objects brighter than $K_s = 14.3$. We adopted the “K20 isophotal fiducial elliptical aperture magnitudes” and selected galaxies not flagged as artifacts (`cc_flg != 'a'`) nor close to large galaxies — thus avoiding spurious fragments in the envelopes of large galaxies (`cc_flg != 'z'`). There is a strong correlation between dust extinction and stellar density, which increases exponentially towards the Galactic Plane. Stellar density is a contaminant factor of the XSC since the reliability of separating stars from extended sources is very sensitive to this quantity (Jarrett et al. 2000). In order to avoid contamination from stars, we have constructed a mask for the 2MASS survey using the HEALPix (Górski et al. 2005) map with $N_{\text{side}} = 256$ and excluding those pixels where the K_s -band extinction $A(K_s) = 0.367 E(B-V) > 0.05$ and $|b| < 20$, which reduces galactic contaminant sources to 2% (Maller et al. 2005). This filtering on galactic extinction reduced the solid angle from $27\,334 \text{ deg}^2$ to $23\,844 \text{ deg}^2$.

The raw magnitudes were corrected for galactic extinction using the reddening map of Schlegel et al. (1998). We also followed Maller et al. and imposed a cut at $K_{\text{lim}}^{2\text{MASS}} = 13.57$ in the corrected magnitudes. The sky distribution of these galaxies is shown as the grey points in Fig. 1. These restrictions produced a sample of 408 618 extended sources which constitute our parent catalogue.

¹ http://irsa.ipac.caltech.edu/cgi-bin/Gator/nph-dd?catalog=fp_xsc

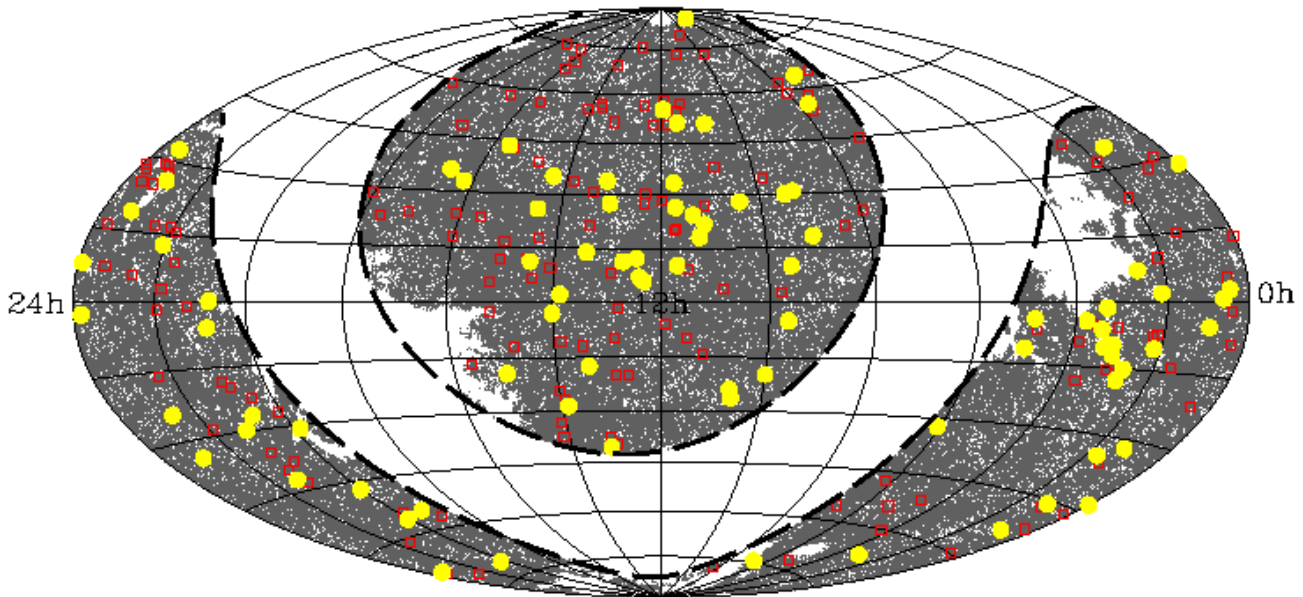


Figure 1. Aitoff projection of galaxies in the 2MASS XSC excluding the region around the Galactic Plane (dashed lines) and regions with high galactic extinction (*background points*). *Open squares* represent the 230 compact groups identified in projection, while *filled circles* are the 85 compact groups after the velocity filter.

3 THE 2MASS CG CATALOGUE

We identify CGs in projection (*p2MCGs*) by using an automated searching algorithm very similar to that defined by Hickson (1982) which is fully described in Díaz-Giménez & Mamon (2010). Briefly, this algorithm identifies as *p2MCGs* those systems that satisfy the following criteria:

- $4 \leq N \leq 10$ (population)
- $\mu_K \leq 23.6 \text{ mag arcsec}^{-2}$ (compactness)
- $\theta_N > 3\theta_G$ (isolation)
- $K_{\text{brightest}} \leq K_{\text{lim}}^{2\text{MASS}} - 3 = 10.57$ (flux limit)

where N is the total number of galaxies whose K -band magnitude satisfies $K < K_{\text{brightest}} + 3$, and $K_{\text{brightest}}$ is the apparent magnitude of the brightest galaxy of the group; μ_K is the mean K -band surface brightness, averaged over the smallest circle circumscribing the galaxy centres; θ_G is the angular diameter of the smallest circumscribed circle, and θ_N is the angular diameter of the largest concentric circle that contains no other galaxies within the considered magnitude range or brighter. Our compactness criterion is set to match that of the HCG, using a mean colour transformation of $K = R - 2.4$ (see appendix A).

In order to speed up this computationally extensive algorithm, we used the subroutines of the HEALPix² package to find neighbours within 5 degrees around each galaxy, and the STRIPACK³ subroutines to compute the centres and radii of the minimum enclosing circles (hereafter CG centres and CG radii, respectively).

Using this algorithm, we found 262 *p2MCGs* in the 2MASS XSC, containing 1158 galaxies. We note, as a curiosity, that $3 \pm 0.5\%$ (binomial errors) of our compact groups with $N > 4$ contain a compact quartet core that also meets all the CG criteria. These are, in fact, CGs within CGs. Note that this percentage is significantly lower than the (6–13)% predicted by Díaz-Giménez & Mamon (2010) from the semi-analytical models (with binomial uncertainty less than 0.5%). Following Díaz-Giménez & Mamon, we always choose the larger CG.

Using the Aladin interactive sky atlas⁴ (Bonnarel et al. 2000) and the Interactive 2MASS image server⁵, we performed a visual inspection of all of these *p2MCGs*. We found that there were 26 galaxy misidentifications in the 2MASS XSC: fragments of larger galaxies (often HII regions) or blends of two galaxies. In other words, since 26 galaxies are misidentifications over a total of 1158, then, for our purposes, the 2MASS XSC turned out to be $97.8 \pm 0.4\%$ reliable. Figure 2 shows a few examples of these misidentifications. In Table 1, we list the 26 objects that belonging to CGs were incorrectly classified as galaxies by 2MASS, and also are quoted the names of their host galaxies. We discarded those CGs of 4 members that hosted one of these galaxies. If a misidentified galaxy belonged to a CG with more than 4 members, then only this galaxy is discarded, and all properties of the CG are recomputed and all the criteria are checked again. In total, 20 groups were discarded because of incorrect 2MASS galaxy identifications.

² <http://healpix.jpl.nasa.gov>

³ http://people.sc.fsu.edu/~burkardt/f_src/stripack/stripack.html

⁴ <http://aladin.u-strasbg.fr/java/nph-aladin.pl>

⁵ <http://irsa.ipac.caltech.edu/applications/2MASS/IM/interactive.html>

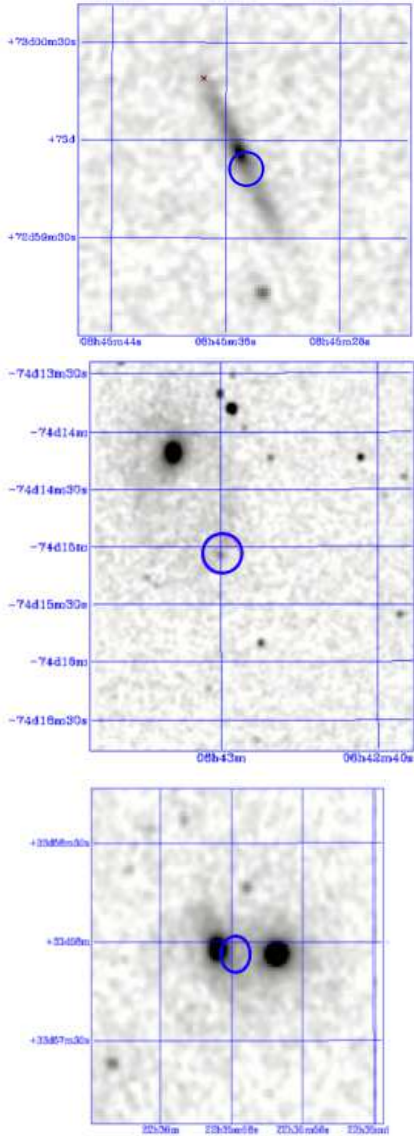


Figure 2. Images in the K_s -band taken from the Interactive 2MASS Image Service showing 2MASS misidentification examples (see Table 1). Circles show the position of these objects in the 2MASS XSC. From top to bottom: 2MASXJ08453453+7259512, 2MASXJ06430003-7415042, 2MASXJ22355791+3357562. In all but the last image, the large galaxy close to the circles also belongs to 2MASS XSC.

Moreover, 2MASS fails to identify some large galaxies that are close to another large galaxy belonging to a CG. For instance, galaxy NGC 7578A does not appear in the 2MASS XSC, while its pair-neighbour, NGC 7578B, does. The same happened with the following 12 galaxies: NGC0414-NED02, IC0590-NED02, NGC 3750, NGC 4783, NGC 5354, NGC 4796, IC 1165 NED02, ESO 284-IG 041 NED02, ESO596-49, LCRSB210329.4-450104, NGC 7318A, NGC 7318B. These 13 missing galaxies among 1158 detected ones make the 2MASS XSC 99% complete for our purposes. Given the lack of K -band magnitudes for these galaxies, we omitted from our sample the 12 CGs containing these 13 galaxies.

Table 1. Objects in the 2MASS XSC that are actually part of larger galaxies

#	Galaxy Name in 2MASS	Main galaxy
1	2MASXJ18533628-5643133	2MASXJ18533694-5643078
2	2MASXJ14080439-3318147	2MASXJ14080314-3318542
3	2MASXJ22355791+3357562	galaxy pair
4	2MASXJ03554380-4222233	2MASXJ03554474-4222024
5	2MASXJ07271181+8544540	2MASXJ07271448+8545162
6	2MASXJ08453453+7259512	2MASXJ08453501+7259560
7	2MASXJ03582336-4428024	2MASXJ03582180-4427585
8	2MASXJ10421741-0022318	2MASXJ10421797-0022365
9	2MASXJ12422507-0702456	2MASXJ12422554-0702364
10	2MASXJ16013973+2121296	2MASXJ16014023+2121106
11	2MASXJ12040147+2013489	2MASXJ12040140+2013559
12	2MASXJ07222530+4916277	2MASXJ07222519+4916427
13	2MASXJ06430003-7415042	2MASXJ06430596-7414103
14	2MASXJ00364578+2134078	2MASXJ00364500+2133594
15	2MASXJ17465074+2045440	2MASXJ17465132+2045400
16	2MASXJ09054355+1820276	2MASXJ09054305+1820226
17	2MASXJ11282505+0924272	2MASXJ11282405+0924279
18	2MASXJ23223215+1153235	2MASXJ23223093+1153332
19	2MASXJ02142411-0722178	2MASXJ02142586-0722064
20	2MASXJ12214093+1129448	2MASXJ12214230+1130118
21	2MASXJ13193834-1242052	2MASXJ13193805-1241562
22	2MASXJ12494210+2653266	2MASXJ12494226+2653312
23	2MASXJ13561035+0514388	2MASXJ13560724+0515169
24	2MASXJ23535429+0757368	2MASXJ23535389+0758138
25	2MASXJ11561045+6031300	2MASXJ11561032+6031211
26	2MASXJ15375266+5923382	2MASXJ15375345+5923304

Table 2. List of acronyms used throughout this work

CG	general compact groups
$p2MCG$	CGs identified in projection from the 2MASS catalogue
$pz2MCG$	$p2MCG$ s whose galaxies have their radial velocities known
$v2MCG$	CGs with 4 or more accordant galaxies (velocity filtered)
$mvCG$	mock velocity-filtered CGs
HCG	Hickson Compact Groups

As a result, we identify 230 $p2MCG$ s in the 2MASS catalogue. In Fig. 1 we show the sky coverage of these groups (*empty squares*). Figure 3 shows images of a few examples of $p2MCG$ s that lie in the SDSS area. Some of the observable properties of the $p2MCG$ s are shown in Fig. 4 and their median values are shown in the second column of Table 4.

A list of acronyms used to refer different samples to be defined throughout this work is provided in Table 2.

4 CROSS-IDENTIFICATION

We compared our sample of CGs to the original HCG sample. We looked for the K -band magnitudes of all the original members of the HCG sample in the 2MASS catalogue. There are 42 HCGs that lie within the studied area (HCG 33 and 34 lie within 20° of the Galactic Plane) and whose brightest galaxy K -band magnitude is brighter than 10.57 (fourth criterion). However, only 20 HCGs have been identified with the $p2MCG$ s in the 2MASS sample, and they are: HCG 4, 7, 10, 15, 16, 21, 22, 23, 25, 40, 42, 51, 58, 86, 87, 88, 93, 97, 99, 100. While 10 of these 20 CGs have the exact same member galaxies, the remaining 10 have galaxies in common but

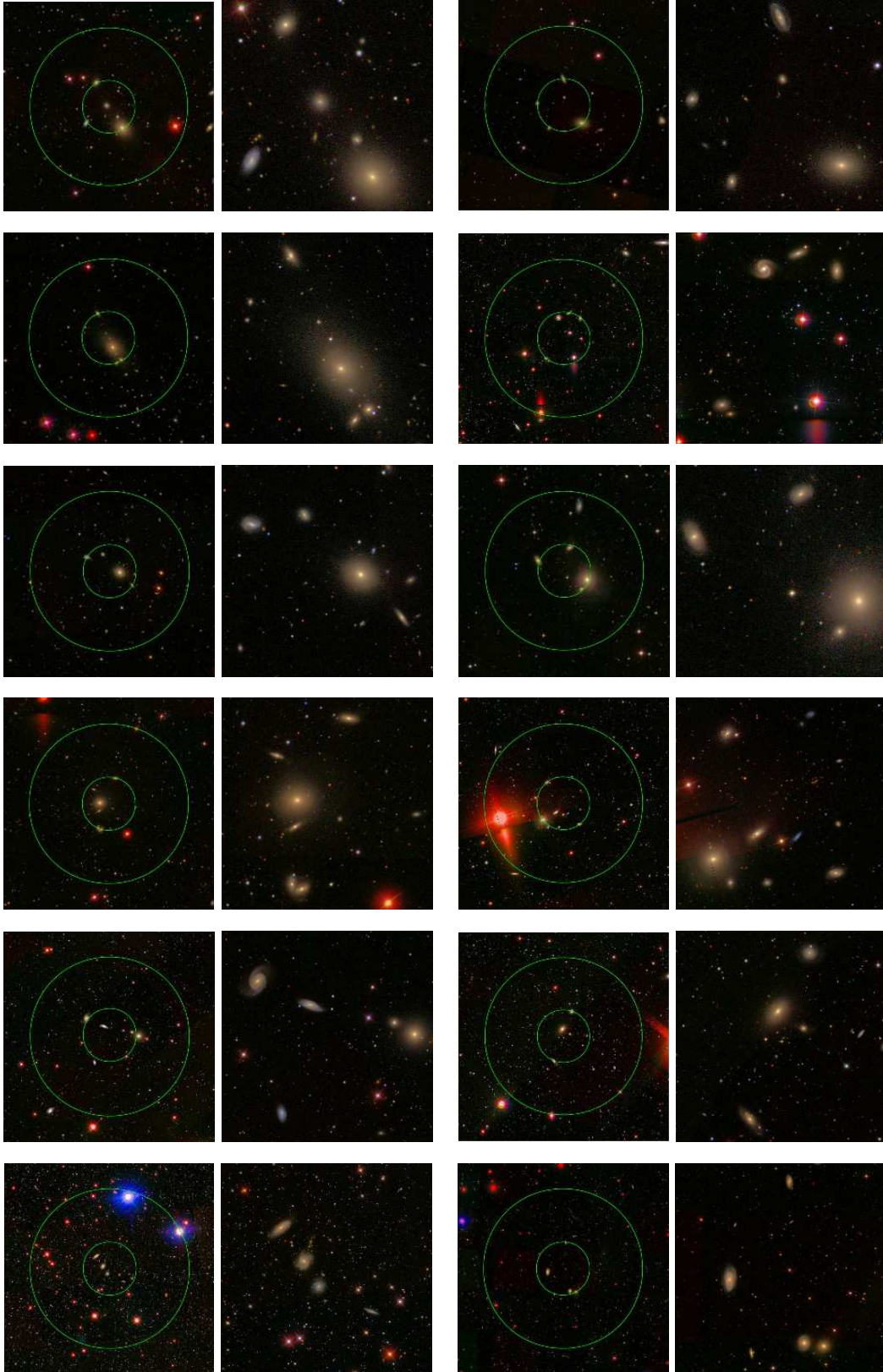


Figure 3. A few examples of $p2MCGs$ that lie within the SDSS area, none of them are already known groups. There are 2 frames per $p2MCG$: the *left frames* show concentric circles which correspond to $1 \theta_G$ and $3 \theta_G$ (see text). The *right frames* are zoomed images which show the regions within θ_G , for each group. According to the notation in Table C1 they are (from left to right and top to bottom): 32, 36, 40, 50, 52, 57, 59, 62, 64, 66, 74, 85.

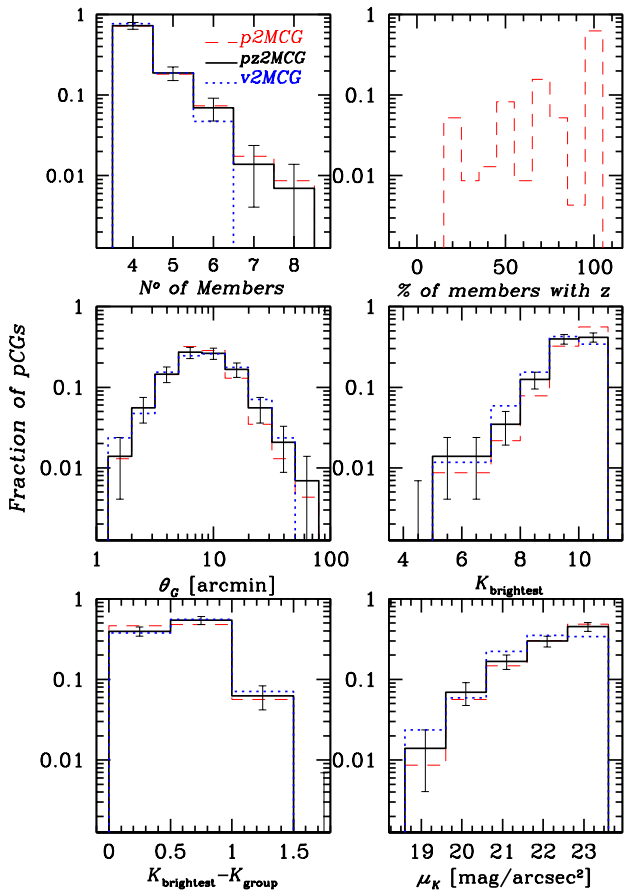


Figure 4. Distributions of observable properties for the CGs identified in projection in the 2MASS XSC: Number of members in the CG (*top left panel*), percentage of members with redshifts available (*top right panel*), group angular diameter (*middle left panel*), K -band apparent magnitude of the brightest galaxy member (*middle right panel*), difference between the brightest galaxy and the total group magnitudes (*bottom left panel*) and mean group surface brightness (*bottom right panel*). *Dashed histograms* correspond to the sample of 230 $p2MCGs$, *solid histograms* correspond to the sample of 144 $p2MCGs$ that have all the redshifts of their galaxies known ($pz2MCGs$), and will be filtered in Sect. 5, while *dotted histograms* correspond to the sample of 85 $v2MCGs$. Error bars correspond to Poisson errors.

are not exactly the same: some groups have more galaxies unidentified by Hickson while others have fewer.

We therefore analysed the reasons why we failed to identify the 22 remaining HCGs among the 42. First, in HCG 68, HCG 92 (Stephan’s quintet) and HCG 94, the 2MASS XSC photometric pipeline blends a pair of galaxies into a single galaxy or only identifies one galaxy of a pair. This then falls into the category of groups discarded due to problematic galaxy identification described in the previous section (in this case, galaxy NGC 5354 for HCG 68, galaxies NGC 7318A and NGC 7318B for Stephan’s quintet, and NGC 7578A for HCG 94). Second, among the 19 remaining unidentified HCGs in our sample, 10 (HCG 5, 56, 57, 61, 65, 74, 90, 91, 96, 98) have less than 4 members within our adopted 2MASS limit of $K = 13.57$, i.e., some of their mem-

bers do not belong to our parent sample. Moreover, HCG 57 also fails the HCG isolation criterion in the R band (Sulentic 1997), while HCG 74 and 96 fail the membership criterion in the R band. Finally, 9 of the HCGs (HCG 11, 19, 30, 41, 44, 48, 53, 62, 67) fail to meet the K -band membership criterion, i.e., have fewer than 4 galaxies with $K - K_{\text{brightest}} < 3$, one of which (HCG 30) also fails to meet this criterion in the R band.

The visual inspection performed using Aladin images has also provided information about other cross-identifications. Only 25% of our $p2MCGs$ have already been completely or partially identified by other authors.

5 VELOCITY-FILTERED COMPACT GROUPS

5.1 Velocity filtering

We searched in the literature for available redshifts for all galaxies in the $p2MCG$ sample, in order to have a sample of concordant groups. First, we correlated the galaxies in the 2MASS extended source catalogue with galaxies in the 2MASS Redshift catalogue (2MRS, Huchra et al. 2012). We have found 561 of our galaxies in $p2MCGs$ in the main catalogue of those authors. Also, another 280 were present in the “extra” catalogue presented by the authors. Then, we looked for the remaining galaxies in the 2M++ redshift compilation (Lavaux & Hudson 2011). We found 9 of the remaining $p2MCG$ galaxies in this catalogue. We also looked for available redshifts in the NED for those galaxies in the $p2MCGs$ that do not belong to the 2MRS nor to 2M++. We have found another 19 redshifts of galaxies in $p2MCGs$. All in all, we find that 869 out of 1020 galaxies (85%) already have measurements of their redshifts available.

A total of 144 (62%) of the $p2MCGs$ have *all* their members with available redshifts, and we hereafter refer to these as $pz2MCGs$. In 20% of the $p2MCGs$ there is one galaxy without available redshift, while in 10% (8%) of the $p2MCGs$ there are two (three or more) galaxies without redshifts.

Fig. 4 shows that the distributions of observable properties of the 144 $pz2MCGs$ are very similar to those for the full sample of $p2MCGs$. Therefore, our subsample of $pz2MCGs$ does not appear biased relative to the full sample of $p2MCGs$.

Using these 144 $pz2MCGs$, we built a sample of velocity-filtered CGs ($v2MCGs$) by following an iterative procedure (see Hickson et al. 1992 and Díaz-Giménez & Mamon 2010). Briefly, after computing the median velocity of the group, we discard the galaxy whose velocity is furthest and at least $\Delta v = 1000 \text{ km s}^{-1}$ from the median. We recompute the velocity median of the remaining galaxies and iterate until all, and at least 4, galaxies lie within Δv from the new median. We then check that the brightest remaining galaxy is brighter than 10.57, and that $\mu_K \leq 23.6 \text{ mag arcsec}^{-2}$. If not, we discard the group.

Our procedure led us to 85 $v2MCGs$ that survive the velocity filtering, and are thus less likely to be contaminated by galaxies in chance projections. The angular distribution of these groups is shown in Fig. 1 (*filled circles*).

Figure 5 shows the properties (see Sect. 5.3 below) of the $v2MCGs$ (solid black histograms). One sees that the sample of $v2MCGs$ appears to be complete up to $K_{\text{group}} \simeq 9$, close

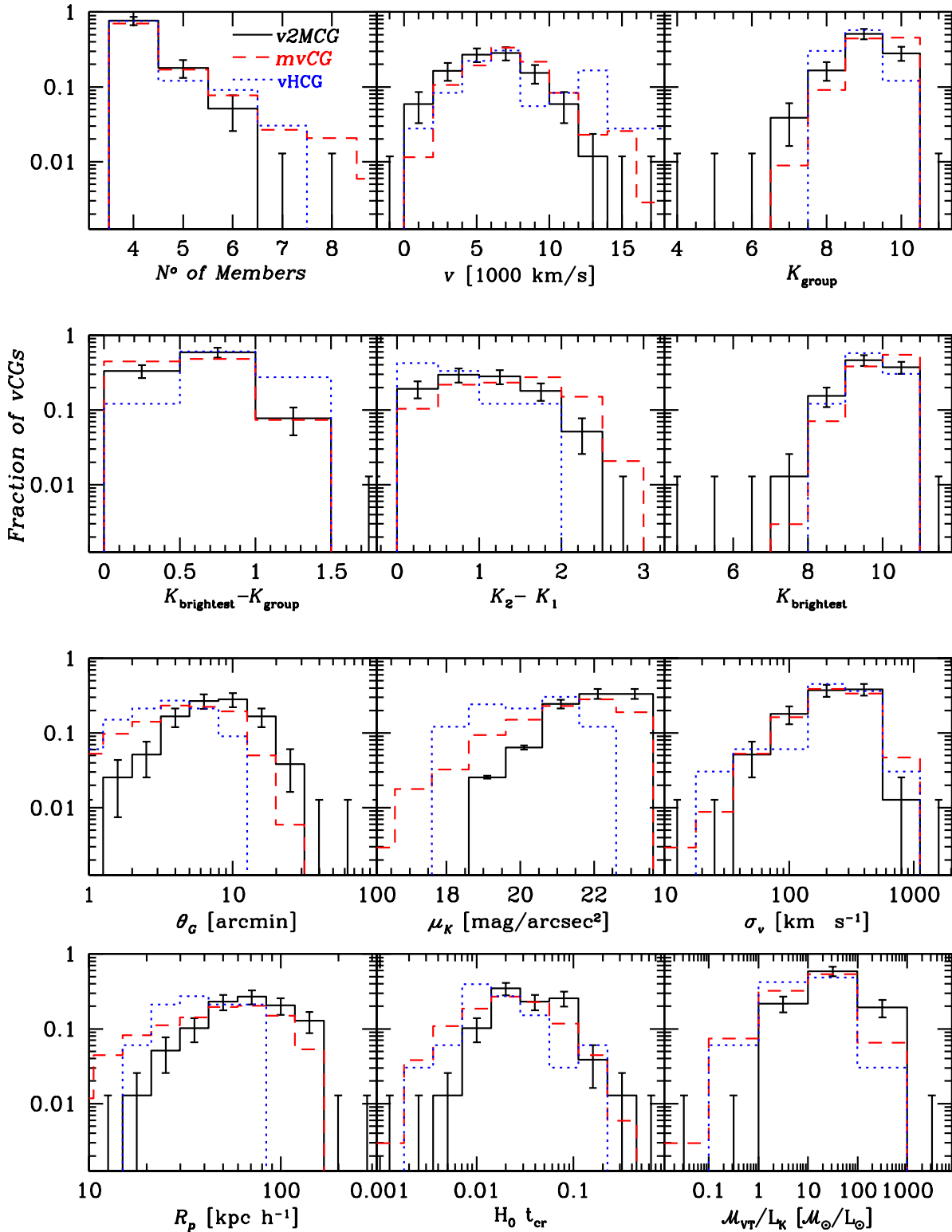


Figure 5. Distributions of properties of the Compact groups after the velocity filtering. All panels are restricted to groups with $\langle v \rangle > 3000 \text{ km s}^{-1}$ except for the median group velocities. *Thick black solid histograms:* $v2MCG$ s; *thin red dashed histograms:* velocity-filtered mock Compact Groups ($mvCG$ s) identified in the r -band from the semi-analytical model of Guo et al. (2011) run on the halos of the MS-II dark matter simulation, and converted to the K -band using $K = R - 2.4 = r - 2.73$ (Table 5); *thin blue dotted histograms:* $vHCG$ are the velocity-filtered HCGs restricted to the limits used in this work and converted to the K -band (sample Hick92/2, Table 5). Error bars correspond to Poisson errors.

to the theoretical limits for quartets ($10.57 - 2.5 \log 4 = 9.06$) and the rarer quintets ($10.57 - 2.5 \log 5 = 8.82$). The $v2MCG$ sample also appears to be fairly complete⁶ to radial velocity of $\sim 6000 \text{ km s}^{-1}$.

Fig. 4 displays a comparison between the sample of projected and filtered CGs. One sees that groups with higher multiplicity, or very large angular size are more prone to be chance alignments along the line of sight.

5.2 Cross-identification

We found that 46% of the $v2MCGs$ were previously (completely or partially) identified by other authors (see last column of Table C1). In particular, the $v2MCGs$ include 16 Hickson compact groups: HCG 7, 10, 15, 16, 21, 23, 25, 40, 42, 51, 58, 86, 88, 93, 97, and 99. Moreover, 52% of the $v2MCGs$ lie in the SDSS area. The median of the properties are quoted in the second column of Table 5.

5.3 Measurement of group properties

The main properties of the $v2MCGs$ are quoted in Table C1. They are:

- Column 1:* Group ID
- Column 2:* Right Ascension of the CG centre
- Column 3:* Declination of the CG centre
- Column 4:* Median radial velocity
- Column 5:* Number of galaxy members in the CG in the range of 3 magnitudes from the brightest member
- Column 6:* Extinction-corrected K -band apparent magnitude of the brightest galaxy
- Column 7:* Extinction-corrected K -band group surface brightness
- Column 8:* Angular diameter of the smallest circumscribed circle
- Column 9:* Median projected separation among galaxies
- Column 10:* Apparent group elongation
- Column 11:* Radial velocity dispersion of the galaxies in the CG
- Column 12:* Dimensionless crossing time
- Column 13:* Mass-to-light ratio in the K -band
- Column 14:* Cross-identification with other group catalogues

The group velocity dispersions, σ_v , are computed using the gapper algorithm following Beers et al. (1990), who found it to be more efficient than standard estimators of dispersion for small samples.⁷ Our values of σ_v are corrected (in quadrature) for the velocity errors.

The extinction corrections in Table C1 refer to the galactic extinction, deduced from Schlegel et al. (1998). We did not correct for internal extinction, because the corrections are usually negligible, except for edge-on spirals where

it is probably of order of 0.2 mag. Moreover, we expect that internal extinction increases not only with the inclination of the disk, but also with disk luminosity (with increasing column density of dust at increasing luminosity for given dust/stars ratio) and metallicity (which controls the dust/stars ratio), as well as on the bulge/disk ratio. Since we lack bulge/disk decomposition for our galaxies, we could have used the internal extinction formulae for 2MASS wavebands of Masters et al. (2003), given as a function of inclination and luminosity. However, their modulation of internal extinction by the luminosity saturates at luminosities of about $0.2 L_*$, whereas it should keep rising because, at increasing luminosity, the column density should increase and the metallicity, hence dust/stars ratio, should also increase. We thus prefer to leave the internal extinction to further analysis.

The physical radii and luminosities assume distances obtained from the redshifts, i.e. we neglect the peculiar velocities of the galaxies relative to the Sun. We could have included a Virgocentric infall model to correct for the peculiar velocity of the Local Group (as given in HyperLEDA⁸, see Terry et al. 2002), but this would not have included the peculiar motions of $v2MCG$ galaxies. The attractor model of Mould et al. (2000) does include the peculiar motions of both the Local Group and the other galaxies, but it misses all the repelling voids. The peculiar velocity flow model of Lavaux et al. (2010) does include the full matter distribution and not just the attractors. But it was built from redshift data and lacks accuracy at distances less than $30 h^{-1} \text{ Mpc}$ because it is not calibrated with available quality distance estimators (Cepheids or surface brightness fluctuations). Since none of the models available satisfied our expectations taking into account all the main velocity components, we decided not to correct for peculiar motions, and we leave this open to further analysis. For peculiar velocities of 300 km s^{-1} , the effects of peculiar motions on distances are less than 10% for galaxies with $cz > 3000 \text{ km s}^{-1}$ (leading to physical size and luminosity errors less than 10% and 20% respectively). For the presentation and analysis of statistical $v2MCG$ properties, we thus restrict our sample to the 78 $v2MCGs$ for which the median group velocity is greater than 3000 km s^{-1} .

We compute the absolute magnitudes of the individual galaxies, assuming that their luminosity distances are all based upon the median group redshift. The cosmology adopted for computing the luminosity distances is the standard cosmology also used in the MS ($\Omega_m = 0.25$, $\Omega_\Lambda = 0.75$). Note that the luminosities are not only corrected for galactic extinction, but are also k -corrected. For computing the k -corrections, we have used the polynomial expressions in terms of redshift and colour $H-K$ given by Chilingarian et al. (2010). The results of the present work depend very little on the details of the k -corrections, since the galaxy samples studied here are from shallow flux-limited surveys, hence limited to low redshifts.

Our dimensionless crossing times are obtained with

$$H_0 t_{\text{cr}} = H_0 \frac{\langle d_{ij}^{3D} \rangle}{\sigma_{3D}} = \frac{100 \pi}{2\sqrt{3}} h \frac{\langle d_{ij} \rangle}{\sigma_v}, \quad (1)$$

⁶ Of course, a flux-limited catalogue is never complete in terms of volume, since galaxies are sampled with increasing minimum luminosity as one goes out to increasing distances, hence the space density of galaxies always decreases (if it were not for fluctuations from the large-scale structure).

⁷ One of us (G.A.M., unpublished) also found the gapper estimate of dispersion to be much less biased for small samples than are other measures.

⁸ <http://leda.univ-lyon1.fr/>

where $\langle d_{ij} \rangle$ is the median of the inter-galaxy projected separations in h^{-1} Mpc. Our mass-to-light ratios are obtained from an application of the virial theorem:

$$\frac{\mathcal{M}_{\text{VT}}}{L} = \frac{3\pi}{2} \frac{(2R_h)\sigma_v^2}{GL}, \quad (2)$$

where $R_h = \langle 1/d_{ij} \rangle^{-1}$ is the harmonic mean projected separation, given the projected separations d_{ij} (see eq. [10–23] of Binney & Tremaine 1987).

The distributions of the main properties of the $v2MCGs$ are shown as solid black histograms in Fig. 5.

5.4 Mock velocity-filtered compact groups

It is instructive to compare the distribution of the properties of $v2MCGs$ with the mock, velocity-filtered compact groups ($mvCGs$) selected on mock galaxy catalogues with the exact same criteria as those described at the top of Sect. 3. We have done this following the prescriptions of Díaz-Giménez & Mamon (2010), who had analysed the $z = 0$ outputs of three different semi-analytical models (SAMs) of galaxy formation (B06, Bower et al. 2006; C06, Croton et al. 2006; and DLB07, De Lucia & Blaizot 2007).

However, since this work, a new SAM has been developed by Guo et al. (2011) (hereafter G11) that reproduces much better, among other things, the $z = 0$ stellar mass function of galaxies. Moreover, Guo et al. have run their SAM not only on the Millennium dark matter simulation, but also on the Millennium-II simulation (MS-II, see Boylan-Kolchin et al. 2009), which has 5 times better space resolution and 125 times better mass resolution. Since CGs are small, space and mass resolution are crucial in producing realistic mock CG catalogues. We have therefore primarily used the outputs of the Guo et al. SAM run on top of the MS-II to build realistic mock light cones to a magnitude limit of $r = 16.3$ (the limit of the 2MASS converted to the SDSS r band) and identify CGs. We have also reanalysed the $z = 0$ output of the SAM by Croton et al. (2006), this time using their K -band magnitudes instead of the R -band ones to a magnitude limit of $K = 13.57$ (the 2MASS completeness limit used throughout this work). We refer to these $mvCGs$ as C06K. Note that, as in Díaz-Giménez & Mamon (2010), we assumed for all SAMs that mock galaxies that are close in projection on the plane of the mock sky would be blended by observers if their angular separation is less than the sum of their angular half-light radii.

Table 3 shows the fraction of $mvCGs$, selected in redshift space as the observed catalogues, that are physically dense in real space with the criteria adopted by Díaz-Giménez & Mamon (2010), who call s the maximum pair separation in real space among the closest subsample of 4 galaxies of the CG or the CG itself for quartets, while S_{\perp} and S_{\parallel} denote the maximum line-of-sight and projected separations of the subsample, respectively. With these notations, the criterion for physically dense groups is that they be physically very small or that they be physically small and not elongated along the line-of-sight: ($s < 100 h^{-1}$ kpc) OR ($s < 200 h^{-1}$ kpc AND $S_{\parallel}/S_{\perp} < 2$). Assuming that the predictions from the SAM can be directly applied to the $v2MCGs$, we predict that between $\sim 53\%$ and $\sim 73\%$ of the sample can be considered as physically dense systems, which means that between ~ 45 and ~ 62 $v2MCGs$ may be truly

dense systems. The remaining $37 \pm 10\%$ of the $mvCGs$ are caused by chance alignments of galaxies along the line-of-sight, usually originating from larger virialised groups (see also Díaz-Giménez & Mamon 2010).

In particular, for the more realistic G11 SAM run on the much better resolved MS-II cosmological dark matter simulation, *two-thirds of the mock velocity-filtered compact groups are physically dense*, while one-third is caused by chance alignments of galaxies along the line-of-sight, mostly within larger virialised groups. So, this better SAM produces a fraction of mock velocity-filtered compact groups that are physically dense that is similar to what Díaz-Giménez & Mamon (2010) had found for the three other SAMs. Comparing the upper and lower rows of Table 3, it is encouraging that the fraction of physically dense $mvCGs$ depends little on the waveband (red or K) used.

6 GENERAL PROPERTIES

It is interesting to compare the properties of the CGs presented in this work to those found in the literature for other CG samples. We downloaded several CG catalogues available at the VizieR service⁹ service of the Centre de Données astronomiques de Strasbourg (CDS), and computed the properties of these groups in the same way we did for our sample of CGs.

6.1 Comparison with photometric catalogues

We retrieved data from VizieR for the following six catalogues: HCG (Hickson 1982), DPOSSCG/03 (Iovino et al. 2003), DPOSSCG/05 (de Carvalho et al. 2005), SDSSCG/04 (Lee et al. 2004), SDSSCG-A/09 (McConnachie et al. 2009), SDSSCG-B/09 (McConnachie et al. 2009). It is important to note that, although we used the membership information from the authors (angular positions and magnitudes), we recomputed all the properties using our own algorithms, to ensure that they were all estimated in the same manner. In this way, we can compare our projected $p2MCG$ catalogue with others in the literature to highlight differences in the searching algorithms and selection criteria.

Table 4 shows the median observable properties and their inter-quartile ranges for the photometric samples of CGs. For a fair comparison among these samples, it is necessary to take into account the different bands in which CGs have been identified in each different catalogue. While our $p2MCGs$ are based upon K -band magnitudes, HCGs have been first identified on POSS-I E plates, whose spectral response is close to the R band, for which the galaxy magnitudes are available. DPOSSCG/03 have SDSS- r band magnitudes, DPOSSCG/05 have R -Gunn magnitudes, and SDSSCG/04/09 have SDSS- r band magnitudes. We assumed that $R = K + 2.4$ (appendix A) and $R = r - 0.33$ (Díaz-Giménez & Mamon 2010) to compare magnitudes in the K and r -band to those in the R -band. Therefore, in Table 4, all magnitudes are converted to the R -band. Table 4 also includes a cleaner subsample of the HCG (Hick82/2)

⁹ <http://vizier.u-strasbg.fr>

Table 3. Mock velocity-filtered compact groups

Parent Λ CDM simulation	MS	MS	MS	MS	MS-II
SAM	B06	C06	DLB07	C06K	G11
Selection band	R	R	R	K	r
$R_{\text{brightest}} \leq 14.44$ & $\mu_R \leq 26$					
Number of $mvCGs$	1952	2011	1251	...	1782
Fraction of physically dense	0.77	0.73	0.58	...	0.69
$K_{\text{brightest}} \leq 10.57$ & $\mu_K \leq 23.6$					
Number of $mvCGs$	379	360	288	486	340
Fraction of physically dense	0.73	0.65	0.53	0.66	0.66

Notes. MS: Millennium Simulation (Springel et al. 2005); MS-II: Millennium-II Simulation (Boylan-Kolchin et al. 2009); B06: Bower et al. (2006); C06: Croton et al. (2006); DLB07: De Lucia & Blaizot (2007); G11: Guo et al. (2011).

Table 4. Median Properties of CGs identified in projection. For a fair comparison, all photometric properties have been translated to the R -band

	$p2MCG$	HCG	DPOSSCG/03	DPOSSCG/05	SDSSCG/04	SDSSCG-A/09	SDSSCG-B/09	HCG
ref.		Hick82	Iov03	deCarv05	Lee04	McCon09	McCon9	Hick82/2
colour eq.	$K = R - 2.4$	$E = R$	$r = R + 0.33$	R	$r = R + 0.33$	$r = R + 0.33$	$r = R + 0.33$	$E = R$
#	230	100	84	459	177	2297	74791	40
θ_G [arcmin]	7.6 ± 2.8	3.1 ± 1.4	0.7 ± 0.1	0.7 ± 0.1	0.4 ± 0.1	1.5 ± 0.4	0.4 ± 0.1	4.4 ± 1.8
$R_{\text{brightest}}$	12.5 ± 0.4	12.7 ± 0.6	16.2 ± 0.2	16.5 ± 0.3	16.8 ± 0.6	15.8 ± 0.5	18.4 ± 0.7	12.3 ± 0.6
R_G	11.9 ± 0.5	11.9 ± 0.6	15.3 ± 0.3	15.6 ± 0.3	16.2 ± 0.5	15.0 ± 0.4	17.6 ± 0.5	11.3 ± 0.6
μ_G [R mag arcsec $^{-2}$]	25.0 ± 0.7	22.8 ± 0.7	23.1 ± 0.3	23.6 ± 0.3	23.2 ± 0.3	24.5 ± 0.6	24.5 ± 0.5	23.2 ± 0.8
$R_{\text{faintest}} - R_{\text{brightest}}$	2.7 ± 0.2	2.4 ± 0.5	1.6 ± 0.3	1.6 ± 0.3	2.7 ± 0.2	1.6 ± 0.5	1.9 ± 0.6	2.2 ± 0.4
$R_{\text{brightest}} - R_G$	0.5 ± 0.2	0.9 ± 0.2	0.9 ± 0.2	0.9 ± 0.1	0.5 ± 0.2	0.9 ± 0.2	0.8 ± 0.2	0.9 ± 0.2

Notes. θ_G : group angular diameter, $R_{\text{brightest}}$: apparent magnitude of the brightest galaxy member in the R -band, R_G : total apparent magnitude of the group (i.e., sum of all members), μ_G : group mean surface brightness, $R_{\text{faintest}} - R_{\text{brightest}}$: difference of apparent magnitudes between the faintest and the brightest galaxy members, $R_{\text{brightest}} - R_G$: difference between the brightest galaxy and the total apparent magnitudes of the groups. Errors are the semi-interquartile ranges. References: Hick82: Hickson (1982); Iov03: Iovino et al. (2003); deCarv05: de Carvalho et al. (2005); Lee04: Lee et al. (2004); McCon09: McConnachie et al. (2009); Hick82/2: Hickson (1982), restricted to $R_{\text{brightest}} \leq 10.57 + 2.4 = 12.97$ and $R_{\text{faintest}} - R_{\text{brightest}} \leq 3$ and with non-isolated groups (Sulentic 1997) removed.

that meets equivalent criteria as the used in this work ($R_{\text{brightest}} \leq 10.57 + 2.4 = 12.97$ and $R_{\text{faintest}} - R_{\text{brightest}} \leq 3$) and for which we omitted 6 HCGs that fail to meet the isolation criterion (Sulentic 1997) (see also *thin dotted blue lines* in Fig. 5).

Table 4 indicates that the $p2MCGs$ have brighter group and first-ranked galaxy apparent magnitudes than those of the other photometric catalogues. This is a consequence of the shallower magnitude limit of the 2MRS spectroscopic survey used here. Restricting the HCG sample to the magnitude limits used here ('Hick82/2'), the median first-ranked galaxy magnitude is slightly brighter than that of the $p2MCGs$. The differences remaining between the $p2MCG$ and Hick82/2 samples arise from the differences between automatic and visual identifications, since the latter by Hickson (1982) were biased (e.g., Díaz-Giménez & Mamon 2010) towards identifying groups with similar galaxies (lower values of $R_{\text{faintest}} - R_{\text{brightest}}$, and higher values of $R_{\text{brightest}} - R_G$), and missing groups close to the compactness limit (lower values of μ_G). On the other hand, the median angular diameter of the $p2MCGs$ is larger than for the other samples, making the surface brightness of our sample the faintest. Moreover, not all the CG catalogues were constructed taking into account our fourth criterion that ensures that group members can be found in a 3 magnitude range from the first-ranked galaxy. In several of the catalogues, the magnitude limit of the sample is sometimes just one or two magni-

tudes fainter than that of the first-ranked galaxy. It is clear that this leads to a bias towards identification of smaller differences between the first-ranked and faintest member of the group, as can be seen, e.g., in the average values of $R_{\text{faintest}} - R_{\text{brightest}}$ of 1.6 for the DPOSS/03/05 and SDSSCG-A/B catalogues.

It is interesting to compare the number of $p2MCGs$ with $\delta > -33^\circ$ and $K_{\text{brightest}} < 10.57$ with the number of HCGs in the same range of magnitudes. We find 193 $p2MCGs$ vs. 40 $pHCGs$ that meet the criteria used in this work translated to the R -band ($K_{\text{brightest}} \leq 10.57$ and $K_i - K_{\text{brightest}} \leq 3$), which means that the completeness of the visually identified HCGs is $\sim 21 \pm 2\%$ (binomial errors) This result is higher than the 14% predicted by Díaz-Giménez & Mamon (2010) from the semi-analytic models of galaxy formation. Moreover, in our analysis of the SAM of Croton et al. (2006), identifying in the deeper R -band mock catalogue and then translating to the K band produces a sample of $mvCGs$ that is only 74% of the size of the $mvCG$ sample directly selected in K . Thus, the incompleteness of the HCG catalogue relative to the 2MCG one is $0.21/0.74 = 0.28$, even higher than the prediction from the SAMs in the R band.

Given that the properties shown in Table 4 are dependent on the distances to the CGs, which are not included in the analysis above, it is also interesting to compare catalogues for which velocity information is available. This is done in the following subsection.

Table 5. Median properties of compact groups after velocity filtering, with radial velocity larger than 3000 km s⁻¹

	<i>v2MCG</i>	HCG	UZC-CG	LCCG	DPOSSII-CG	HCG	<i>mvCG</i>
ref.		Hick92	Foc02	Allam00	Pom12	Hick92/2	G11
colour eq.	$K = R - 2.4$	$E = R$	$B = R + 1.7$	R	$B = R + 1.7$	$E = R$	$r = R + 0.33$
#	78	67	49	17	33	33	326
θ_G [arcmin]	7.7 ± 3.1	2.5 ± 1.3	11.8 ± 4.2	1.0 ± 0.3	—	3.6 ± 1.5	4.8 ± 2.8
$R_{\text{brightest}}$	12.2 ± 0.4	12.7 ± 0.6	12.6 ± 0.5	16.1 ± 0.4	—	12.2 ± 0.5	12.4 ± 0.4
R_G	11.5 ± 0.5	11.9 ± 0.7	11.3 ± 0.5	15.1 ± 0.3	—	11.3 ± 0.5	11.8 ± 0.4
μ_G [mag arcsec ⁻²]	24.5 ± 0.7	22.7 ± 0.6	25.5 ± 0.6	23.9 ± 0.6	—	22.7 ± 0.9	23.9 ± 1.1
$R_{\text{faintest}} - R_{\text{brightest}}$	2.5 ± 0.3	2.1 ± 0.5	1.2 ± 0.4	1.2 ± 0.5	—	2.2 ± 0.4	2.7 ± 0.2
$R_{\text{brightest}} - R_G$	0.6 ± 0.2	0.9 ± 0.2	1.2 ± 0.4	1.1 ± 0.2	—	0.8 ± 0.2	0.6 ± 0.2
$R_2 - R_1$	1.0 ± 0.4	0.6 ± 0.4	0.4 ± 0.4	0.5 ± 0.3	—	0.6 ± 0.4	1.3 ± 0.5
$L_R / 10^{10} [h^{-2} L_\odot]$	6.7 ± 1.7	11.5 ± 5.1	7.1 ± 2.6	3.0 ± 0.7	4.2 ± 1.0	12.6 ± 5.1	6.7 ± 2.2
v [km s ⁻¹]	6361 ± 1680	9248 ± 2976	6287 ± 1380	23599 ± 3715	32321 ± 5522	7042 ± 3191	7023 ± 1471
σ_v [km s ⁻¹]	237 ± 105	262 ± 93	298 ± 99	243 ± 103	194 ± 55	271 ± 78	248 ± 115
$\langle d_{ij} \rangle$ [h^{-1} kpc]	86 ± 24	43 ± 15	132 ± 34	42 ± 5	31 ± 6	47 ± 15	59 ± 28
r_p [h^{-1} kpc]	65 ± 25	34 ± 12	108 ± 27	35 ± 6	—	36 ± 12	48 ± 23
b/a	0.43 ± 0.17	0.37 ± 0.17	0.47 ± 0.19	0.37 ± 0.16	—	0.37 ± 0.15	0.40 ± 0.18
$H_0 t_{\text{cr}}$	0.032 ± 0.024	0.013 ± 0.008	0.039 ± 0.024	0.014 ± 0.008	0.018 ± 0.005	0.016 ± 0.008	0.020 ± 0.017
$\mathcal{M}_{\text{VT}}/L_R$ [$h \mathcal{M}_\odot/L_\odot$]	116 ± 42	42 ± 28	235 ± 193	117 ± 76	94 ± 34	39 ± 20	53^{+91}_{-32}
T_1	0.51 ± 0.06	1.27 ± 0.17	1.04 ± 0.15	1.10 ± 0.27	—	1.15 ± 0.22	0.46 ± 0.02
T_2	0.70 ± 0.06	1.01 ± 0.10	1.13 ± 0.11	1.10 ± 0.19	—	0.98 ± 0.13	0.59 ± 0.02
P_S	3×10^{-4}	0.19	0.53	0.86	—	0.31	0
P_{KS}^{1-2}	9×10^{-4}	(0.40)	0.09	(0.93)	—	(0.08)	5×10^{-10}
P_{KS}^{2-3}	(0.90)	(0.69)	(0.23)	(0.93)	—	0.25	(0.38)

Notes. All the photometric properties have been translated to the R -band to allow comparison among catalogues. #: number of CGs with 4 or more concordant members; θ_G : group angular diameter; $R_{\text{brightest}}$: apparent magnitude of the brightest galaxy member in the R -band; R_G : total apparent magnitude; μ_G : group mean surface brightness; $R_{\text{faintest}} - R_{\text{brightest}}$: difference of apparent magnitudes between the faintest and the brightest galaxy members; $R_{\text{brightest}} - R_G$: difference between the brightest galaxy and the total apparent magnitudes; $R_2 - R_1$: difference of absolute magnitudes between the brightest and the second brightest galaxy of the group (same statistics for difference in absolute R -band magnitudes, after including k -corrections from Chilingarian et al. 2010 and Poggianti 1997); L_G : total luminosity of the CG; v : group median radial velocity; σ_v : group gapper (Wainer & Thissen 1976) velocity dispersion, corrected for galaxy velocity errors (assumed to be 40 km s⁻¹ when unavailable); $\langle d_{ij} \rangle$: median inter-galaxy separation; r_p : group radius (of smallest circumscribed circle); b/a : apparent elongation of the group (1=round); $H_0 t_{\text{cr}}$: dimensionless crossing time (eq. [1]); $\mathcal{M}_{\text{VT}}/L_R$: mass-to- R -light ratio from the virial theorem (eq. [2]); T_1 and T_2 : Tremaine-Richstone statistics (Tremaine & Richstone 1977, eq. [3]); P_S : probability of greater anti-correlation of luminosity with position occurring by chance (Spearman rank correlation test); P_{KS}^{1-2} : probability of greater difference in distributions of positions between 1st and 2nd ranked galaxies, occurring by chance (Kolmogorov-Smirnov test); P_{KS}^{2-3} : same for difference in distribution of positions between 2nd and 3rd ranked galaxies. Numbers in parentheses for these three quantities indicates reverse luminosity segregation (brighter galaxies further out). Errors are the semi-interquartile ranges, except for T_1 and T_2 , where they are standard deviations computed with 10 000 bootstraps. **References:** Hick92: Hickson et al. (1992); Foc02: Focardi & Kelm (2002); Allam00: Allam & Tucker (2000); Pom12: Pompei & Iovino (2012), restricted to isolated (classes A, CH and CP) with at least 4 accordant redshifts; Hick92/2: Hickson et al. (1992), restricted to isolated groups (following Sulentic 1997) and restricted to $R_{\text{brightest}} \leq 10.57 + 2.4 = 12.97$ and $R_{\text{faintest}} - R_{\text{brightest}} \leq 3$; G11: mock compact groups extracted (following the method of Díaz-Giménez & Mamon 2010) from the mock galaxy catalogue of Guo et al. (2011) applied to the MS-II (Boylan-Kolchin et al. 2009) cosmological N body simulation.

6.2 Comparison with observed and mock spectroscopic catalogues

We retrieved galaxy data from VizieR for the following compact group catalogues with velocity information: HCG (Hickson et al. 1992), UZC-CG (Focardi & Kelm 2002), and LCCG (Allam & Tucker 2000). We also extracted the group information from the new DPOSSII-CG catalogue (Pompei & Iovino 2012). We, then, proceeded to compare those samples to our *v2MCG* sample, after transforming again all samples to the R band with colours $R-K = 2.4$ (Appendix A), $B = R + 1.7$ (Prandoni et al. 1994) and $r = R + 0.33$ (Díaz-Giménez & Mamon 2010). We have applied k -corrections to the different catalogues using the morphology-based corrections of Poggianti (1997) (UZC-CG and LCCG) or colour-based corrections of

Chilingarian et al. (2010) (2MCG, HCG).¹⁰ We have included the cleaner Hick92/2 sub-sample (see Sect. 6.1) now velocity-filtered, and also the sample of *mvCGs* that we extracted from G11's SAM. The median values of the properties of the velocity-filtered CGs are quoted in Table 5 as well as their semi-interquartile ranges.

6.2.1 Space density

We computed the space density within the median distance of the sample ($60 h^{-1} \text{ Mpc}$) as $\eta_{60} = 3N(<60)/(60^3 \Omega)$. For the *v2MCGs* the space density is $8.0 \times 10^{-5} h^3 \text{ Mpc}^{-3}$.

¹⁰ We did not apply k -corrections to DPOSSII-CG because of lack of galaxy information, and we corrected their crossing time definition to ours ($\pi^2/9 \simeq 1.2$ times greater).

In comparison, the space density for the Hick92/2 sample is $1.86 \times 10^{-5} h^3 \text{Mpc}^{-3}$, i.e. that the space density of the $v2MCGs$ is ~ 4.3 times larger. From the G11 SAM, the space density of the $mvCGs$ is $12.7 \times 10^{-5} h^3 \text{Mpc}^{-3}$, which means that it almost doubles (~ 1.6) that of the $v2MCGs$.

6.2.2 Distribution of group properties

In Fig. 5, we show the distribution of group properties for our $v2MCGs$ (solid histograms), $vHCGs$ (blue dotted histograms), and the $mvCGs$ from G11 (thin dashed red histograms). The comparison with other SAMs can be found in the Appendix B¹¹. Table 5 shows that the nearest samples are the UZC-CG and $v2MCG$ samples, although the HCG sample restricted to the criteria used in this work also includes only the nearest groups. The two nearby CG samples present the largest projected radii, median inter-particle distances, dimensionless crossing times and mass-to-light ratios. The five CG samples have similar median properties (to within the semi-interquartile ranges), except for T_1 and T_2 (see below). In particular, the median velocity dispersions for the different catalogues are fairly similar, ranging from 194 to 295 km s^{-1} .

Our sample has the highest median crossing time of all samples, while the HCG has the lowest crossing time. The latter result is probably caused by the lack of HCGs near the surface brightness limit (Walke & Mamon 1989; Prandoni et al. 1994; Díaz-Giménez & Mamon 2010).

There is a good general agreement between the predictions from the SAM and the observations from 2MASS. But some differences stand out: in comparison with the $mvCGs$, the $v2MCG$ sample lacks groups of high-multiplicity (as checked with a KS test on the full N distributions), very low velocity dispersion, small angular and physical sizes, high surface brightness, and low \mathcal{M}_{VT}/L_K , but has too many groups that lie at low redshifts, or that are globally bright (K_{group}) or with bright 1st-ranked galaxy ($K_{\text{brightest}}$).

Our identification of more $v2MCGs$ at low redshifts than predicted by the SAM might be a sign that our local neighbourhood ($cz < 2000 \text{ km s}^{-1}$) is denser than on average, perhaps thanks to the presence of the Virgo and Fornax clusters, or conversely that the observer we placed in a random position in the cosmological box turned out to be in an underdense region (for small volumes one might expect that cosmic variance is than Poisson variance). This excess of nearby CGs would explain our excess of $v2MCGs$ with large angular size and of low surface brightness. However, we also find an excess in physical radii, which suggests that we suffer more from galaxy blending than we accounted for in our $mvCGs$.

6.2.3 Apparent group elongations

Using projected Cartesian coordinates on the plane of the sky, we calculated the 2-dimensional shape tensor, whose

¹¹ Given that the numbers of $mvCGs$ from the different SAMs are typically 4 times the number of $v2MCGs$, the relative uncertainties on their differential distribution is half of those of the $v2MCGs$, and are not shown in the Figure, for clarity.

Table 6. Group (quartets) velocity dispersion vs. apparent elongation

Catalogue	r	P_S	$\langle \sigma_v^{\text{chain}} \rangle$	$\langle \sigma_v^{\text{round}} \rangle$	P_{KS}
			(km s ⁻¹)		
$v2MCG$	0.01	0.95	204	188	0.50
HCG (Hick92/2)	0.20	0.33	149	284	0.19
$mvCG$ -G11	0.11	0.11	208	272	0.09
$mvCG$ -C06	0.01	0.85	240	209	0.94
$mvCG$ -B06	0.04	0.54	227	240	0.75
$mvCG$ -DLB07	0.02	0.81	290	274	0.99
$mvCG$ -C06K	0.10	0.10	240	280	0.10

Notes. The samples are those listed in Table 5, hence limited to $v > 3000 \text{ km s}^{-1}$, but also restricted to quartets ($N = 4$). The columns are r : Spearman rank correlation coefficient; P_S : probability of stronger correlation than r occurring by chance; $\langle \sigma_v^{\text{chain}} \rangle$ and $\langle \sigma_v^{\text{round}} \rangle$: median group velocity dispersions for chain-like ($b/a < 0.3$) and round ($b/a > 0.5$) groups, respectively; P_{KS} : probability of greater difference between velocity dispersion distributions for groups with $b/a < 0.3$ and $b/a > 0.5$ occurring by chance (Kolmogorov-Smirnov statistic).

eigenvalues are related to the major (a) and minor (b) semi-axes. We measure the elongations of the groups in the plane of the sky as the ratio between the major and minor semi-axes (b/a). Lower values of b/a imply more elongated systems on the plane of the sky. Table 5 indicates that the apparent group elongations are similar between all catalogues.

Using a different technique to measure group apparent elongations, Tovmassian et al. (1999) found that group velocity dispersions were significantly smaller (by 28%, with large uncertainty) in chain-like groups than in rounder ones, which we hereafter denote the Tovmassian effect. Now, geometrical considerations imply that the distribution of group shapes depends on the number of its members (e.g. Hickson et al. 1984), with low multiplicity groups being on average more elongated. Since velocity dispersion scales as mass, which scales as number, one would then expect from the geometrical considerations that high velocity dispersion groups will be rounder, as found by Tovmassian et al.. However, these authors also noticed trends for triplets, quartets and quintets separately, and while none were statistically significant, they argued that the probability that all three trends were present (albeit weak) was significant.¹²

Table 6 shows our analysis of the velocity dispersion and apparent elongations of the *quartets* (thus avoiding any geometrical source for the Tovmassian effect). In the $v2MCG$ sample, there is no correlation between group apparent elongation and velocity dispersion, while in the cleaned HCG sample (Hick92/2) and the mock (from G11's SAM) CGs, there are weak correlations between σ_v and b/a , but they are not statistically significant. However, for the Hick92/2 and G11 samples, the median velocity dispersion of the chain-like ($b/a < 0.3$) groups is much smaller than that of the round ($b/a > 0.5$) groups, while the opposite behaviour is observed for the $v2MCGs$. Yet, the effect is not significant in the $v2MCG$, only marginally significant in the mock sam-

¹² Tovmassian et al. (1999) did not present any statistical tests for the separate multiplicities, nor for the combination of the larger mean velocity dispersions for the triplets, quartets and quintets.

ple, while the Hick92/2 sample, with only 13 quartets, is too small to provide a statistically significant difference in the distributions of velocity dispersions between chain-like and round groups. We note that if we increase the Hick92/2 sample to groups with galaxy magnitudes $R < 14.97$ (instead of $R < 12.97$), we end up with 41 HCG quartets, for which the rank correlation coefficient between apparent elongation and velocity dispersion is now $r = 0.29$, yielding a correlation with 97% significance. However, for this deeper Hick92/2 sample, the difference in the distributions of velocity dispersions for chain-like and round quartets is still not statistically significant.

6.2.4 Bright end of the luminosity function

Tremaine & Richstone (1977) devised two simple, yet powerful statistics, based on Cauchy-Schwarz inequalities, to test whether the first-ranked galaxies in groups and clusters were consistent with one or several arbitrary luminosity functions. They defined T_1 and T_2 as follows:

$$T_1 = \frac{\sigma(M_1)}{\langle M_2 - M_1 \rangle} \quad T_2 = \frac{1}{\sqrt{0.677}} \frac{\sigma(M_2 - M_1)}{\langle M_2 - M_1 \rangle} \quad (3)$$

where the averages are means and where $\sigma(M_1)$ and $\sigma(M_2 - M_1)$ are the standard deviations of the absolute magnitude of the brightest galaxy (M_1) and difference in absolute magnitude ($M_2 - M_1$) between the second- and first-ranked galaxies. Values of T_1 and T_2 lower than unity imply that the first-ranked group galaxies are abnormally bright at the expense of the second-ranked galaxy. N -body simulations indicate that galaxy mergers within physically dense groups rapidly reduce the values of T_1 and T_2 below 0.7 (Mamon 1987a). T_1 and T_2 are biased low for samples with small number of groups, $N < 50$ (Mamon 1987b).

In Table 5, we find that the $v2MCG$ sample displays T_1 and T_2 significantly lower than unity: $T_1 = 0.51 \pm 0.06$ and $T_2 = 0.70 \pm 0.06$ (1σ errors from 10 000 bootstraps). We also find such low values in our mock $mvCG$ sample from G11 as well as in our four other $mvCG$ samples.

However, none of the other observed CG samples display low values of T_1 and T_2 . In particular, the HCG samples show $T_1 \approx 1.2$ and $\simeq T_2 \simeq 1.0$. It appears that Hickson (1982) missed CGs with very dominant galaxies (Prandoni et al. 1994; Díaz-Giménez & Mamon 2010), thus creating a spuriously high T_1 . Indeed, Table 5 shows that $R_2 - R_1$ (hence, the difference in absolute magnitudes) has a median value of 1.0 for the $v2MCG$ sample (1.3 for the $mvCG$ s), but only 0.6 for the HCG samples (the means are similar). Still, part of the difference in T_1 values is caused by the larger standard deviations of 1st-ranked absolute magnitudes in the HCG samples (0.8) in comparison with the $v2MCG$ (0.53) and G11- $mvCG$ (0.58) samples.

In comparison, Loh & Strauss (2006) found $T_1 = 0.75 \pm 0.1$ and $T_2 = 0.86 \pm 0.1$ in nearby rich SDSS clusters dominated by Luminous Red Galaxies (LRGs), while Lin et al. (2010) recently found $T_1 = 0.70 \pm 0.01$ and $T_2 = 0.96 \pm 0.01$ in luminous SDSS clusters, but $T_1 = 0.84 \pm 0.01$ and $T_2 = 0.94 \pm 0.01$ for low luminosity ones.

We can also quantify how significant are the deviations of T_1 and T_2 from unity using a Monte-Carlo technique (see also Lin et al. 2010). We built mock CGs by adopting the absolute magnitudes of the first-ranked $v2MCG$ s and adding to

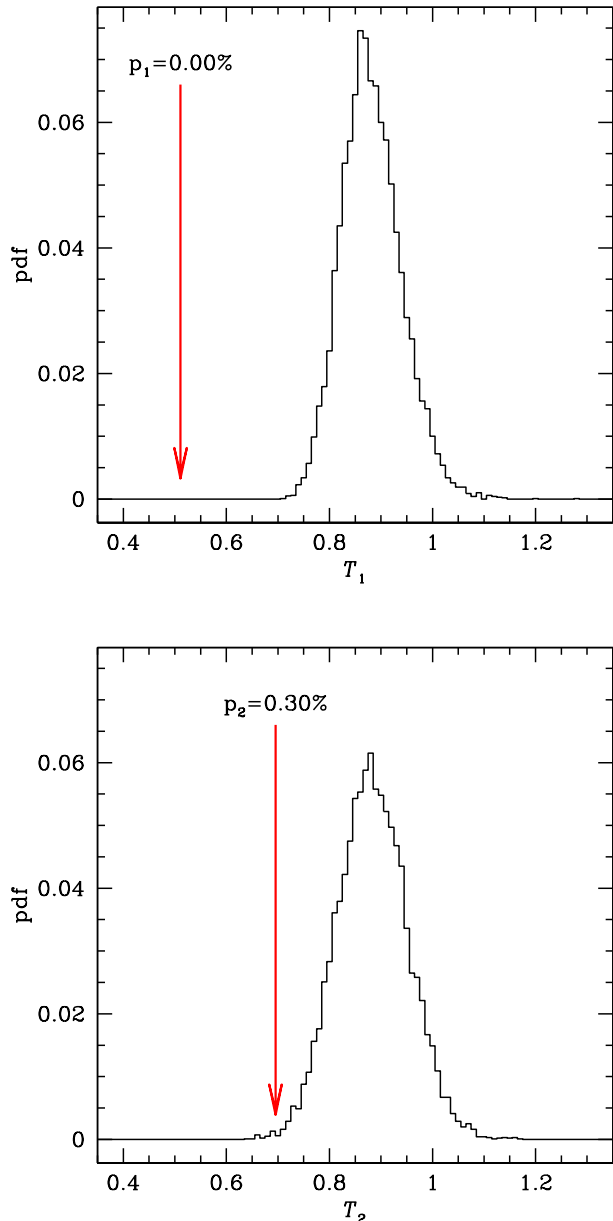


Figure 6. Distributions of Tremaine-Richstone statistics for 10 000 Monte-Carlo realisations. Vertical arrows indicate the values observed in the $v2MCG$ catalogue ($v > 3000 \text{ km s}^{-1}$).

them the absolute magnitudes of galaxies chosen at random from the 2MRS catalogue, but with 3 limitations: 1) in the same range of redshifts (velocities 1000 km s^{-1} from that of the first-ranked); 2) absolute magnitudes, M_K , in the range of the group: $M_K^{\text{grp}-1} \leq M_K \leq M_K^{\text{grp}-1} + 3$, where $M_K^{\text{grp}-1}$ is the absolute magnitude of the first-ranked group member; 3) positions more than 5 degrees from the group (in Declination only for a faster run). The velocity criterion ensures that the flux limit of 2MRS is properly handled, while the position criterion ensures that a first-ranked galaxy is not duplicated in its mock group. In the end we thus generate mock CGs with the same multiplicity function and distribution of most luminous absolute magnitudes. We did not

consider a surface brightness threshold on our Monte-Carlo groups (assuming that the galaxies are located in the same positions as in the observed sample), because this would increase the discrepancy between the observed values of T_1 and T_2 with those from our Monte-Carlo samples. Indeed, since we start with the brightest group galaxy, if we enforced a minimum group surface brightness, we would tend to reject groups with only one luminous member, hence leading us to lower differences between second and first-ranked absolute magnitudes, and therefore larger values of T_1 and T_2 . We compute T_1 and T_2 for this mock sample of CGs and iterate to build a total of 10 000 samples.

The distribution of T_1 and T_2 for the 10 000 mock catalogues can be seen in Fig. 6. Let p_i be the fraction of Monte-Carlo realisations that have T_i as low as the observed value. We found $p_1 = 0$ (i.e. $p_1 < 0.01\%$) and $p_2 = 0.3 \pm 0.06\%$, i.e. none of our mocks reached values of T_1 and T_2 both as low as observed in $v2MCGs^{13}$.

All this confirms that *the v2MCG is the only observed compact group sample that has differences between first- and second-ranked absolute magnitudes that are inconsistent with random sampling of luminosity functions*, in agreement with the expectations from cosmological simulations.

6.2.5 Luminosity segregation

In the standard galaxy formation model used for SAMs, the brightest group galaxies are centrally located (see Skibba et al. 2011 for the quantification and limits of this idea). Indeed, N-body simulations of virialised dense groups show that such luminosity segregation rapidly sets in (Mamon 1987a). Moreover, the two-body relaxation times in dense groups of galaxies, of order of the number of galaxies times the orbital time, both of which are small, are expected to be much smaller than the age of the Universe, hence galaxies should exchange their orbital energies and reach equipartition on short timescales. If CGs are caused by chance alignments, then one does not expect to witness such luminosity segregation. Mamon (1986) measured luminosity segregation in HCGs, using the exact same technique as he used in the simulations: stacking the groups and searching for a correlation (with the Spearman rank test) between the fraction of group luminosity in the galaxy (hereafter, fractional luminosity) versus the projected distance relative to the group centroid (unweighted barycentre) in units of the median of these distances per group (hereafter, normalised radial coordinate). The absence of luminosity segregation in HCGs, measured in this fashion, produced for him another argument that HCGs were heavily contaminated by chance alignments.

Here, we performed the same analysis on the different observed and mock samples of CGs. We first found that $v2MCGs$ show significant anti-correlation between fractional

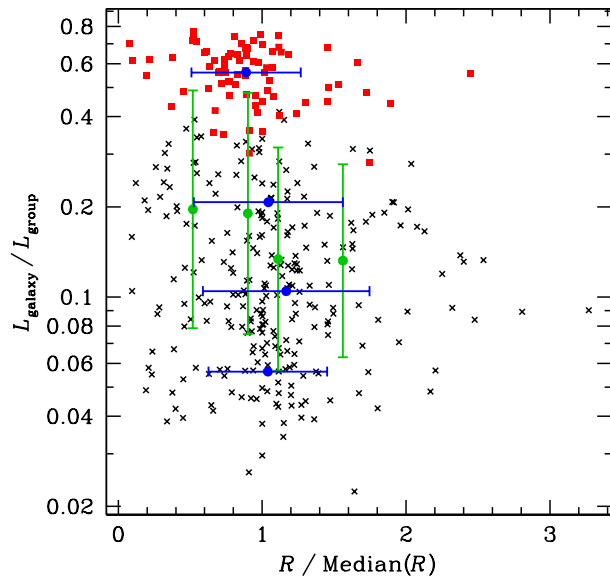


Figure 7. Luminosity segregation (fractional luminosity in group vs. normalised radial coordinate relative to unweighted barycentre) in the $v2MCG$ sample (restricted to $v > 3000 \text{ km s}^{-1}$). The red squares indicate the first-ranked galaxies, while the black crosses show the other group galaxies. The horizontal and vertical error bars show the standard deviations in equal number subsamples of normalised radius and fractional luminosity, respectively. Despite the large scatter, the rank correlation coefficient is $r = -0.19$ and has only a probability 3×10^{-4} of occurring by chance.

luminosity and normalised distance: Spearman rank correlation $r = -0.19$. According to the Spearman rank correlation test, an anti-correlation at least as strong as this observed one has less than 0.1% probability of arising by chance (see Table 5). This is also the case in the mock $mvCG$ sample. One may argue that SAMs have luminosity segregation within them by construction, since in SAMs, galaxies form at the centre of a halo. But none of the other observed CG samples show any significant sign of luminosity segregation, and this is not just a case of poorer statistics, as the correlation coefficient between fractional luminosities and normalised distances in the $v2MCG$ is much more negative than in all other observed samples.

We also compared the stacked distributions of normalised distances between first- and second-ranked galaxies, as well as between second- and third-ranked galaxies, using the Kolmogorov-Smirnov (KS) test. As seen in the last two rows in Table 5, in $v2MCGs$, the first-ranked galaxy is significantly more centrally located than the second-ranked galaxies: according to the KS test, the probability that this would occur by chance is again less than 0.1%. This is also seen in the $mvCGs$, while no such significant trends are seen in the other group catalogues (including the HCG). Hence, *The v2MCG is the only CG sample to show that the most luminous galaxies are significantly more centrally located, in accordance with the mock CGs from SAMs, and contrary to what has been observed in all other CG sample.*

Interestingly, there are no statistically significant signs for different distributions of normalised distances between

¹³ Note that Lin et al. (2010) also considered the compatibility of the distribution of observed values of T_1 and T_2 of clusters using bootstrap resampling with the predicted distribution obtained with mocks. This incorrectly accounts twice for the finite sample. One should either use bootstraps to provide error bars on the observed T_1 and T_2 and compare to the mean prediction of the mocks or conversely compare the observed T_1 and T_2 without error bars to the distribution of the mocks, but not do both.

second- and third-ranked galaxies. In other words, while the first-ranked galaxies are in general more centrally located than the second-ranked, the latter are not more centrally located than the third-ranked. This lack of luminosity segregation among the non-brightest galaxies may occur because tides from the parent group potential, may limit the sizes hence luminosities of the galaxies as they approach the central one (whose central location renders it immune to such tides). Then, the second most luminous galaxy will preferentially lie at the outskirts, while the third ranked one, will tend to lie closer because of this tidal limitation. Therefore, for the non-brightest galaxies, group tides may cancel the effect of luminosity segregation.

Figure 7 illustrates the luminosity segregation in the $v2MCG$ sample. The fractional group luminosities appear to be enhanced within the median projected distance from the group centroid (i.e. abscissae smaller than unity). However, the normalised distances are only smaller in the galaxies in the 25% highest quartile of fractional luminosity, which roughly corresponds to the first-ranked galaxies.

7 CONCLUSIONS AND DISCUSSION

In this work we have catalogued a new sample of CGs from the 2MASS survey and we have compared them with existing CG samples.

Following the criteria defined by Hickson (1982), we have identified 230 CGs in projection in the K -band covering 23844 deg^2 . This catalogue has well defined criteria which produced an homogeneous sample useful to perform statistical analyses on it. 25% of them (57 CGs) were previously identified in other catalogues as compact groups, triplets of galaxies or interacting galaxies. A total of 144 $p2MCGs$ have *all* their members with redshifts available in the literature, and among them 85 groups have 4 or more accordant galaxies, which makes this catalogue the largest sample of CGs with 4 or more spectroscopically confirmed members. The percentage of groups with accordant galaxies (59%) is slightly lower than that obtained from the HCG sample (67%), and very similar to the predicted by Díaz-Giménez & Mamon (2010) from the semi-analytical models of Bower et al. (2006) and De Lucia & Blaizot (2007).¹⁴

As a side note, we have now built additional mock CG catalogues using the Croton et al. (2006) SAM in the K -band and the Guo et al. (2011) SAM in the r band, where the latter was run on the Millennium-II Simulation, which has 512 times the mass resolution of the Millennium Simulation. For both samples, we found that two-thirds of the mock CGs were physically dense systems of at least 4 galaxies of accordant magnitudes, while the remaining third was caused by chance alignments of galaxies along the line-of-sight, mostly within larger virialised groups, confirming similar conclusions of Díaz-Giménez & Mamon (2010).

In comparison with other CG catalogues, the $v2MCG$ catalogue presented in this work is one of the nearest and brightest samples of CGs, although these CGs have larger projected radii and interparticle separations.

The $v2MCG$ does not show any significant correlation for quartets between apparent elongation and velocity dispersion nor significantly larger velocity dispersion in round groups relative to chain-like groups, contrary to what Tovmassian et al. (1999) claimed in HCGs.

The $v2MCG$ is the only CG sample to display significantly large differences between second- and first-ranked absolute magnitudes (from Tremaine-Richstone statistics) as well as centrally located first-ranked galaxies, both in agreement with mock $mvCGs$, but in sharp contrast with all other observed velocity-filtered CG samples.

Galaxy mergers are an obvious way to decrease T_1 and T_2 (Mamon 1987a), and we cannot think of any other physical mechanism that may cause both T_1 and T_2 to be significantly smaller than unity in a group catalogue.

One major difference of our sample with others is that ours has many more groups with dominant galaxies accounting for over half the total luminosity. While this increases the gap between first and 2nd-ranked magnitudes, we found that our sample also has a small standard deviation of first-ranked absolute magnitudes, which enhances the significance of the Tremaine-Richstone T_1 statistic.

Why don't we find significant magnitude gaps and luminosity segregation in the other CG samples? It is clear that in his visually search for CGs, Hickson (1982) missed groups with dominant galaxies (Prandoni et al. 1994; Díaz-Giménez & Mamon 2010 and Table 5). Could those $v2MCGs$ in common with $vHCGs$ have weaker signs of magnitude gaps and luminosity segregation? One expects that if mergers cause the magnitude gap, the masses, i.e. stellar masses, of the galaxies are the crucial variable. Similarly, if luminosity segregation is produced by dynamical friction or by energy equipartition from two-body relaxation, the galaxy (stellar) masses should be the important variable. Therefore, the magnitude gaps and luminosity segregation should be weaker in the R band, where the luminosity is less a measure of stellar mass than in the K -band.

Unfortunately, we have only 14 groups in common, among which 10 (HCG 7, 10, 23, 25, 40, 58, 86, 88, 93, 99)¹⁵ have exactly the same galaxies. For these 10 groups, we find $T_1 = 0.68 \pm 0.24$ and $T_2 = 0.87 \pm 0.24$ in the K band, while in the R band we find values greater than unity: $T_1 = 1.75 \pm 1.69$ and $T_2 = 1.33 \pm 0.39$. So, indeed, the K -band luminosities are more sensitive than their R -band counterparts to the magnitude gap, but given the bootstrap errors, the large differences in T_1 and T_2 between R and K -based absolute magnitudes are not statistically significant (for T_2 the difference is roughly 1σ , while it is much less for T_1). On the other hand, luminosity segregation is not seen in either waveband: worse it is inverted, with the brightest galaxy on average further away from the group centroid than the 2nd-brightest galaxy.

The other two CG samples, UZC-CG and LCCG, are based upon Friends-of-Friends (LCCG) or similar (UZC-CG) algorithms, both with velocity linking length of 1000 km s^{-1} . Such a velocity link is much more liberal than imposing that the velocities all lie within 1000 km s^{-1} from the median as done in Hickson et al. (1992) and here. Indeed, according to Table 5, the median velocity dispersion

¹⁴ For the SAM of Guo et al. (2011), we find that 70% of mock CGs found in projected space survive the velocity filtering.

¹⁵ and with slightly variations: HCG 15, 16, 51, 97.

of UZC-CG groups of 4 or more galaxies is 295 km s^{-1} , i.e. 25% greater than in our sample. This suggests that the UZC-CG sample is more contaminated by chance alignments of galaxies along the line-of-sight (as Mamon 1986 had suggested for the HCG sample) than is our sample. Moreover, the UZC-CG has a liberal linking length on projected distances of $200 h^{-1} \text{ kpc}$, making these groups not so compact (as can be checked by their low mean group surface brightness as seen in Table 5). Finally, the UZC-CG is based upon Zwicky’s visually estimated magnitudes, which may carry rms errors as large as 0.5 mag, thus washing out in part the effects of the magnitude gap and luminosity segregation.

On the other hand, the LCCG sample (again, restricted to groups with at least 4 members) has a very similar median velocity dispersion to our sample (and a similar median mass-to-light ratio). Note that the linking length for projected distances of the LCCG is only $50 h^{-1} \text{ kpc}$, i.e. 4 times less than in UZC-CG. The problem with the LCCG is that its parent catalogue (the LCRS, Shectman et al. 1996) is a collection of two samples with $16.0 < R < 17.3$ and $15.0 < R < 17.7$. Thus the magnitude range is very restricted. Hence, it is not a surprise that $\langle M_2 - M_1 \rangle$ is half our value (Table 5), leading to $T_1 > 1$ and $T_2 > 1$.

What does this tell us on the nature of the groups in the different CG samples? Over 25 years ago, Mamon (1986) found $T_1 = 1.16$ and no signs of luminosity segregation in the largest sample then available of 41 velocity-filtered HCGs with at least 4 members. This was in sharp contrast with the low values of T_1 and significant luminosity segregation he was finding in coalescing dense groups (Mamon 1987a). This provided him with two arguments (among several) to conclude that most HCGs were caused by chance alignments of galaxies within larger groups (Mamon 1986). As confirmed here with the SAM by Guo et al. (2011), roughly two-thirds of mock CGs are physically dense (Díaz-Giménez & Mamon 2010 and Table 3 above). The statistically large magnitude gaps and luminosity segregation in both the observed $v2MCG$ s and the mock $mvCG$ s suggest that Mamon (1986) was misled by the bias of the HCG sample against large gaps into concluding that most of them were not physically dense.

So the $v2MCG$ appear to be mostly *bona fide* physically dense groups. But can we conclude that the other CG samples are dominated by chance alignments? Díaz-Giménez & Mamon (2010) attempted to build sample of mock HCGs that include the same biases as they had measured by comparing with the three SAMs that they had built mock CGs from. They found that the same fraction (if not slightly higher) of the mock (biased) HCGs were physically dense. The nature of the groups in other CG samples could be studied in similar ways, using mock CG samples from cosmological galaxy formation simulations, mimicking their selection criteria and observational select effects.

Could the lack of HCGs with strongly dominant brightest galaxies prevent the visibility of luminosity segregation? We performed KS tests to compare the distribution of relative positions of 1st and 2nd-ranked group members for subsamples split between those dominated by 1st-ranked members (‘Dom’) and those with galaxies of more comparable luminosities (‘Non-Dom’), making our splits at the median magnitude difference $\langle M_2 - M_1 \rangle$. We performed this analysis for the HCG and $v2MCG$ samples as well as for

Table 7. Luminosity segregation split by magnitude gap

Catalogue	subsample	N	P_{KS}
$v2MCG$	Dom	39	2.9×10^{-7}
$v2MCG$	Non-Dom	39	(3.9%)
$vHCG$	Dom	17	67%
$vHCG$	Non-Dom	16	(6.6%)
$mvCG$ -G11	Dom	163	1.2×10^{-11}
$mvCG$ -G11	Non-Dom	163	1.0%
$mvCG$ -C06K	Dom	223	4.0×10^{-9}
$mvCG$ -C06K	Non-Dom	225	0.4%

Notes. Dom and Non-Dom subsamples are those with $M_2 - M_1$ above and below the median value of the full sample, respectively. N is the number of groups in the subsample. P_{KS} is the KS probability that a difference in the distributions of normalised distances to the non-weighted group centre is greater than ‘observed’ by chance. Values of P_{KS} given in parentheses denote reverse luminosity segregation: the 2nd-ranked galaxy is more centrally located than the first-ranked.

the C06K and G11 $mvCG$ samples. Table 7 shows that indeed luminosity segregation is much stronger for all catalogues in the Dom subsamples, and statistically significant in all of them except the $vHCG$. Surprisingly, while the Non-Dom subsamples of the two mock CG samples display much weaker, but still statistically significant luminosity segregation, the Non-Dom subsamples of both the $v2MCG$ and $vHCG$ catalogues display *reversed luminosity segregation*: the 2nd-ranked galaxy is more centrally located than the (slightly more luminous) first-ranked galaxy. We can only see one explanation for this reverse luminosity segregation, if it occurs in wavebands bluer than K : late-type galaxies that are second-ranked in stellar mass, hence not centrally located, can end up more luminous (thanks to their efficient star formation) than early-type galaxies of slightly higher stellar mass. However the effect is also present in the K -selected $v2MCG$, and with even greater statistical significance (96.1% vs. 93.7% confidence for the Non-Dom CGs of the $v2MCG$ and $vHCG$ catalogues, respectively). So, we can only explain this marginal effect as a statistical fluke.

Nevertheless, the absence of luminosity segregation in the HCG catalogue could be consistent with their physical reality because the sample is too small to detect the weak luminosity segregation expected from the mocks. Moreover, if the reverse luminosity segregation for Non-Dom groups is real, then the lack of groups with very dominant galaxies in the HCG (caused by the visual selection bias) would cause the Non-Dom groups to cancel the luminosity segregation of the Dom groups.

In conclusion, the $v2MCG$ sample has numerous advantages over other CG samples:

- (i) It is the largest available sample of velocity-filtered groups of at least 4 members of comparable luminosity (3 mag, i.e. factor 16).
- (ii) It has an isolation criterion (in contrast with other CG samples except for the HCG).
- (iii) It is automatically extracted (contrary to the HCG).
- (iv) It has a well-defined magnitude limit (which the HCG sample does not).
- (v) It is deep enough (which some may find surprising given the shallowness of its parent 2MASS catalogue) to have a selection on brightest galaxy magnitude, so as to ensure that

all groups can span the maximum allowed magnitude gap of 3.

(vi) It is selected by stellar mass (K band), which is expected to be a better tracer for magnitude gaps and luminosity segregation (among other things).

(vii) It is the only sample to show statistical signs of mergers (magnitude gaps) and luminosity segregation, expected in physically dense groups (in contrast with all other CG samples).

The last point implies that the $v2MCG$ is the only CG sample for which one is reasonably sure that it is dominated by physically dense groups. For all these reasons, the $v2MCG$ appears to be the sample one ought to study in depth to probe the effects on galaxies of this unique environment of 4 galaxies of comparable luminosity lying close together in real space.

As a next step in this project, we are in the process of measuring redshifts for the members for which no spectra are available, and we are continuing our statistical studies of the $v2MCGs$ and their galaxies.

8 ACKNOWLEDGMENTS

We thank the anonymous referee for helpful comments that improved this work.

We dedicate this article to John P. Huchra (1948–2010), who among his numerous contributions to astronomy, played a crucial role in obtaining redshifts for the galaxies in groups in general and HCGs in particular. We thank Roya Mohayaee and Guilhem Lavaux for useful discussions on peculiar velocities and Igor Chilingarian on k -corrections and internal extinctions.

This publication makes use of data products from the Two Micron All Sky Survey, which is a joint project of the University of Massachusetts and the Infrared Processing and Analysis Centre/California Institute of Technology, funded by the National Aeronautics and Space Administration and the National Science Foundation. This research has made use of VizieR and Aladin at the Centre de Données astronomiques de Strasbourg (CDS). This research made use of the “K-corrections calculator” service available at <http://kcor.sai.msu.ru/>. An SM version (`kcorr_Chilingarian`) is available at ftp://ftp.iap.fr/from_users/gam/SOFT/gam_macros. The Millennium and Millennium II Simulation databases used in this paper and the web application providing online access to them were constructed as part of the activities of the German Astrophysical Virtual Observatory. This work was partially supported by Consejo de Investigaciones Científicas y Técnicas de la República Argentina (CONICET) and Fundação de Amparo à Pesquisa do Estado do São Paulo (FAPESP). CMdO acknowledges financial support from FAPESP and CNPq.

REFERENCES

Allam S. S., Tucker D. L., 2000, *Astronomische Nachrichten*, 321, 101
 Arp H., 1966, *ApJS*, 14, 1

Arp H. C., Madore B. F., 1987, *A Catalogue of Southern Peculiar Galaxies and Associations 2 volume set*, Arp, H. C. & Madore, B. F., ed.
 Barnes J., 1985, *MNRAS*, 215, 517
 Barton E., Geller M., Ramella M., Marzke R. O., da Costa L. N., 1996, *AJ*, 112, 871
 Beers T. C., Flynn K., Gebhardt K., 1990, *AJ*, 100, 32
 Binney J., Tremaine S., 1987, *Galactic Dynamics*. Princeton, NJ, Princeton University Press, 1987
 Bode P. W., Cohn H. N., Lugger P. M., 1993, *ApJ*, 416, 17
 Bonnarel F., Fernique P., Bienaymé O., Egret D., Genova F., Louys M., Ochsenbein F., Wenger M., Bartlett J. G., 2000, *A&AS*, 143, 33
 Borthakur S., Yun M. S., Verdes-Montenegro L., 2010, *ApJ*, 710, 385
 Bower R. G., Benson A. J., Malbon R., Helly J. C., Frenk C. S., Baugh C. M., Cole S., Lacey C. G., 2006, *MNRAS*, 370, 645
 Boylan-Kolchin M., Springel V., White S. D. M., Jenkins A., Lemson G., 2009, *MNRAS*, 398, 1150
 Cardelli J. A., Clayton G. C., Mathis J. S., 1989, *ApJ*, 345, 245
 Carnevali P., Cavaliere A., Santangelo P., 1981, *ApJ*, 249, 449
 Chilingarian I. V., Melchior A.-L., Zolotukhin I. Y., 2010, *MNRAS*, 405, 1409
 Coziol R., Ribeiro A. L. B., de Carvalho R. R., Capelato H. V., 1998, *ApJ*, 493, 563
 Crook A. C., Huchra J. P., Martimbeau N., Masters K. L., Jarrett T., Macri L. M., 2008, *ApJ*, 685, 1320
 Croton D. J., Springel V., White S. D. M., De Lucia G., Frenk C. S., Gao L., Jenkins A., Kauffmann G., Navarro J. F., Yoshida N., 2006, *MNRAS*, 365, 11
 de Carvalho R. R., Gonçalves T. S., Iovino A., Kohl-Moreira J. L., Gal R. R., Djorgovski S. G., 2005, *AJ*, 130, 425
 de la Rosa I. G., de Carvalho R. R., Vazdekis A., Barbuy B., 2007, *AJ*, 133, 330
 de la Rosa I. G., de Carvalho R. R., Zepf S. E., 2001, *AJ*, 122, 93
 De Lucia G., Blaizot J., 2007, *MNRAS*, 375, 2
 Deng X.-F., He J.-Z., Ma X.-S., Jiang P., Tang X.-X., 2008, *Central European Journal of Physics*, 6, 185
 Diaz-Giménez E., Mamon G., 2010, *MNRAS*, 409, 1227
 Focardi P., Kelm B., 2002, *A&A*, 391, 35
 Górski K. M., Hivon E., Banday A. J., Wandelt B. D., Hansen F. K., Reinecke M., Bartelmann M., 2005, *ApJ*, 622, 759
 Guo Q., White S., Boylan-Kolchin M., De Lucia G., Kauffmann G., Lemson G., Li C., Springel V., Weinmann S., 2011, *MNRAS*, 413, 101
 Hickson P., 1982, *ApJ*, 255, 382
 Hickson P., Kindl E., Auman J. R., 1989, *ApJS*, 7, 687
 Hickson P., Mendes de Oliveira C., Huchra J. P., Palumbo G. G., 1992, *ApJ*, 399, 353
 Hickson P., Ninkov Z., Huchra J., Mamon G., 1984, in *Clusters and Groups of Galaxies*, Mardirossian F., Giuricin G., Mezzetti M., eds., Reidel, Dordrecht, pp. 367–373
 Huchra J. P., Macri L. M., Masters K. L., Jarrett T. H., Berlind P., Calkins M., Crook A. C., Cutri R., Erdoğan P., Falco E., George T., Hutcheson C. M., Lahav O., Mader J., Mink J. D., Martimbeau N., Schneider S., Skrutskie

- M., Tokarz S., Westover M., 2012, ApJS, 199,
- Iovino A., 2002, AJ, 124, 2471
- Iovino A., de Carvalho R., Gal R., Odewahn S., Lopes P., Mahabal A., Djorgovski S., 2003, AJ, 125, 1660
- Jarrett T. H., Chester T., Cutri R., Schneider S., Skrutskie M., Huchra J. P., 2000, AJ, 119, 2498
- Karachentsev I. D., 1972, Astrofizicheskie Issledovaniia Izvestiya Spetsial'noj Astrofizicheskoi Observatorii, 7, 3
- Karachentsev V. E., Karachentsev I. D., Lebedev V. S., 1988, Astrofizicheskie Issledovaniia Izvestiya Spetsial'noj Astrofizicheskoi Observatorii, 26, 42
- Karachentseva V. E., Karachentsev I. D., 2000, Astronomy Reports, 44, 501
- Lavaux G., Hudson M. J., 2011, MNRAS, 416, 2840
- Lavaux G., Tully R. B., Mohayaee R., Colombi S., 2010, ApJ, 709, 483
- Lee B. C., Allam S. S., Tucker D. L., Annis J., Johnston D. E., Scranton R., Acebo Y., Bahcall N. A., Bartelmann M., Böhringer H., Ellman N., Grebel E. K., Infante L., Loveday J., McKay T. A., Prada F., Schneider D. P., Stoughton C., Szalay A. S., Vogeley M. S., Voges W., Yanny B., 2004, AJ, 127, 1811
- Lin Y.-T., Ostriker J. P., Miller C. J., 2010, ApJ, 715, 1486
- Loh Y.-S., Strauss M. A., 2006, MNRAS, 366, 373
- Maller A. H., McIntosh D. H., Katz N., Weinberg M. D., 2005, ApJ, 619, 147
- Mamon G. A., 1986, ApJ, 307, 426
- , 1987a, ApJ, 321, 622
- , 1987b, in Bulletin of the American Astronomical Society, Vol. 19, Bulletin of the American Astronomical Society, pp. 651–651
- , 1989, A&A, 219, 98
- , 1992, ApJ, 401, L3
- , 1994, Ap&SS, 217, 237
- , 2008, A&A, 486, 113
- Masters K. L., Giovanelli R., Haynes M. P., 2003, AJ, 126, 158
- McConnachie A. W., Patton D. R., Ellison S. L., Simard L., 2009, MNRAS, 395, 255
- Mendes de Oliveira C., Hickson P., 1991, ApJ, 380, 30
- Moles M., del Olmo A., Perea J., Masegosa J., Marquez I., Costa V., 1994, A&A, 285, 404
- Mould J. R., Huchra J. P., Freedman W. L., Kennicutt Jr. R. C., Ferrarese L., Ford H. C., Gibson B. K., Graham J. A., Hughes S. M. G., Illingworth G. D., Kelson D. D., Macri L. M., Madore B. F., Sakai S., Sebo K. M., Silberman N. A., Stetson P. B., 2000, ApJ, 529, 786
- Poggianti B. M., 1997, A&A, 122, 399
- Pompei E., Iovino A., 2012, A&A, 539, A106
- Ponman T. J., Bourner P. D. J., Ebeling H., Böhringer H., 1996, MNRAS, 283, 690
- Prandoni I., Iovino A., MacGillivray H. T., 1994, AJ, 107, 1235
- Ramella M., Geller M. J., Pisani A., da Costa L. N., 2002, AJ, 123, 2976
- Rose J. A., 1977, ApJ, 211, 311
- Schlegel D. J., Finkbeiner D. P., Davis M., 1998, ApJ, 500, 525
- Seyfert C. K., 1948, AJ, 53, 203
- Shectman S. A., Landy S. D., Oemler A., Tucker D. L., Lin H., Kirshner R. P., Schechter P. L., 1996, ApJ, 470, 172
- Skibba R. A., van den Bosch F. C., Yang X., More S., Mo H., Fontanot F., 2011, MNRAS, 410, 417
- Skrutskie M. F., Cutri R. M., Stiening R., Weinberg M. D., Schneider S., Carpenter J. M., Beichman C., Capps R., Chester T., Elias J., Huchra J., Liebert J., Lonsdale C., Monet D. G., Price S., Seitzer P., Jarrett T., Kirkpatrick J. D., Gizis J. E., Howard E., Evans T., Fowler J., Fullmer L., Hurt R., Light R., Kopan E. L., Marsh K. A., McCallon H. L., Tam R., Van Dyk S., Wheelock S., 2006, AJ, 131, 1163
- Springel V., White S. D. M., Jenkins A., Frenk C. S., Yoshida N., Gao L., Navarro J., Thacker R., Croton D., Helly J., Peacock J. A., Cole S., Thomas P., Couchman H., Evrard A., Colberg J., Pearce F., 2005, Nature, 435, 629
- Stephan M., 1877, MNRAS, 37, 334
- Sulentic J. W., 1997, ApJ, 482, 640
- Terry J. N., Paturel G., Ekholm T., 2002, A&A, 393, 57
- Torres-Flores S., Mendes de Oliveira C., Amram P., Plana H., Epinat B., Carignan C., Balkowski C., 2010, ArXiv e-prints: 1003.0345
- Tovmassian H. M., Martinez O., Tiersch H., 1999, A&A, 348, 693
- Tremaine S. D., Richstone D. O., 1977, ApJ, 212, 311
- Tzanavaris P., Hornschemeier A. E., Gallagher S. C., Johnson K. E., Gronwall C., Immler S., Reines A. E., Hoversten E., Charlton J. C., 2010, ApJ, 716, 556
- Verdes-Montenegro L., Yun M. S., Williams B. A., Huchtmeier W. K., Del Olmo A., Perea J., 2001, A&A, 377, 812
- Vorontsov-Velyaminov B. A., Noskova R. I., Arkhipova V. P., 2001, Astronomical and Astrophysical Transactions, 20, 717
- Wainer H., Thissen D., 1976, Psychometrika, 41, 9
- Walke D. G., Mamon G. A., 1989, A&A, 225, 291
- White R. A., Bliton M., Bhavsar S. P., Bornmann P., Burns J. O., Ledlow M. J., Loken C., 1999, AJ, 118, 2014

APPENDIX A: TRANSFORMATION FROM μ_R TO μ_K

In the visual search performed by Hickson (1982) on the photographic plates of POSS-I, he established a cutoff in surface brightness of $\mu_E = 26$ mag arcsec⁻². The POSS-I *E* band roughly corresponds to the more familiar Cousins *R* band. As the galaxy database used for our search is selected in the *K_s* band, we converted the original limit of Hickson (1982) to a corresponding one for *K* magnitudes. The *R*–*K* colours¹⁶ of galaxies depend on their luminosity (colour-luminosity relation) and morphology (e.g. Red Sequence vs. Blue Cloud).

We cross-identified the SDSS DR7 model *g* and *r* magnitudes, A_g and A_r extinctions, and redshifts with the 2MASS XSC *K*20 isophotal *J* and *K* magnitudes, with a maximum separation of 2'' between the positions of the galaxies in the two catalogues. We corrected the 2MASS magnitudes for galactic extinction using the A_g values of SDSS, assuming $A_g/A_V = 1.256$, $A_r/A_V = 0.798$, and $A_{K_s}/A_V = 1.16$ from spline fits of $\log A_\lambda$ vs. $\log \lambda$ tabulated by Cardelli et al.

¹⁶ we drop the 's' subscript on the *K_s* band for clarity.

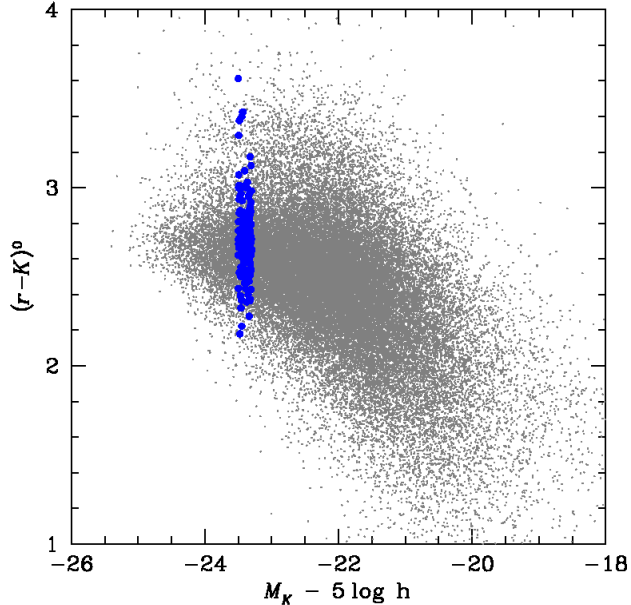


Figure A1. Colour-luminosity relation for SDSS-2MASS matches. The *grey points* show all 45974 non-flagged galaxies with $0.005 < z < 0.05$, $13 < r < 17.77$, $K < 13.57$, while the *blue points* use the additional criteria $M_K - 5 \log h = -23.40 \pm 0.10$ and $z = 0.020 \pm 0.005$.

(1989) and $A_J/A_V = 0.282$ directly from their table. We then k -corrected the SDSS r and 2MASS K_s extinction-corrected magnitudes using the redshifts and extinction-corrected $g-r$ (SDSS) and the $J-K_s$ (2MASS) colours using the transformations of Chilingarian et al. (2010). This enabled us to derive extinction- and k -corrected $(r-K)^0$ colours.

In a first pass, we adopt the conservative $(r-K)^0=2.33$, which, with $(r-R)^0=0.33$ (Díaz-Giménez & Mamon 2010) yields $\mu_K \leq 24 \text{ mag arcsec}^{-2}$. Once we extract the $p2MCGs$ and then the velocity-filtered $v2MCGs$ with this compactness limit, we find that the mean galaxy luminosity in our $v2MCGs$ is $M_K = -23.40 + 5 \log h$ and our median $v2MCG$ mean velocity is 5927 km s^{-1} , corresponding to $z = 0.020$. In a second pass, we consider the $(r-K)^0$ colours for the 45974 galaxies among the 326320 SDSS-2MASS matches, with SDSS `zWarn=0`, $13 < r < 17.77$, and 2MASS artifact flag `cc_flg=0` and both J and K confusion flags, respectively `j_flg_k20fe` and `k_flg_k20fe`, equal to 0 (grey points of Fig. A1). Restricting these matched galaxies to those with $M_K - 5 \log h = -23.40 \pm 0.10$ and $z = 0.020 \pm 0.005$ (large blue points in Fig. A1) yields a median $(r-K)^0$ of 2.72 ± 0.04 (assuming that the error on the median is $1.253 \sigma / \sqrt{N}$, valid for large Gaussian distributions) for 164 galaxies.

With $(r-R)^0=0.33$, this yields $(R-K)^0=2.39$. For clarity, we therefore assume $R = K + 2.4$ and adopt a compactness limit of $\mu_K = 23.6$. The $v2MCGs$ obtained with this new compactness limit have very similar median redshifts (now 1.5% larger), although the median R -band group luminosities are now one-third lower (mainly because of the additional 0.4 magnitude correction from K to R).

APPENDIX B: COMPARISON WITH DIFFERENT SAMs

In Fig. 5, we showed the comparison of the distributions of velocity-filtered CG properties between the $v2MCG$ and the $mvCG$ (from Guo et al. 2011 run on the MS-II) samples. In Fig. B1, we show this comparison for several SAMs: *Left upper panels: mvCGs* identified from Croton et al. (2006)'s SAM in the K -band, *Right upper panels: mvCGs* identified from Croton et al. (2006)'s SAM in the R -band, *Left lower panels: mvCGs* identified from Bower et al. (2006)'s SAM in the R -band, *Right lower panels: mvCGs* identified from De Lucia & Blaizot (2007)'s SAM in the R -band.

APPENDIX C: PROPERTIES OF CGs AFTER VELOCITY-FILTERING IN THE 2MASS XSC

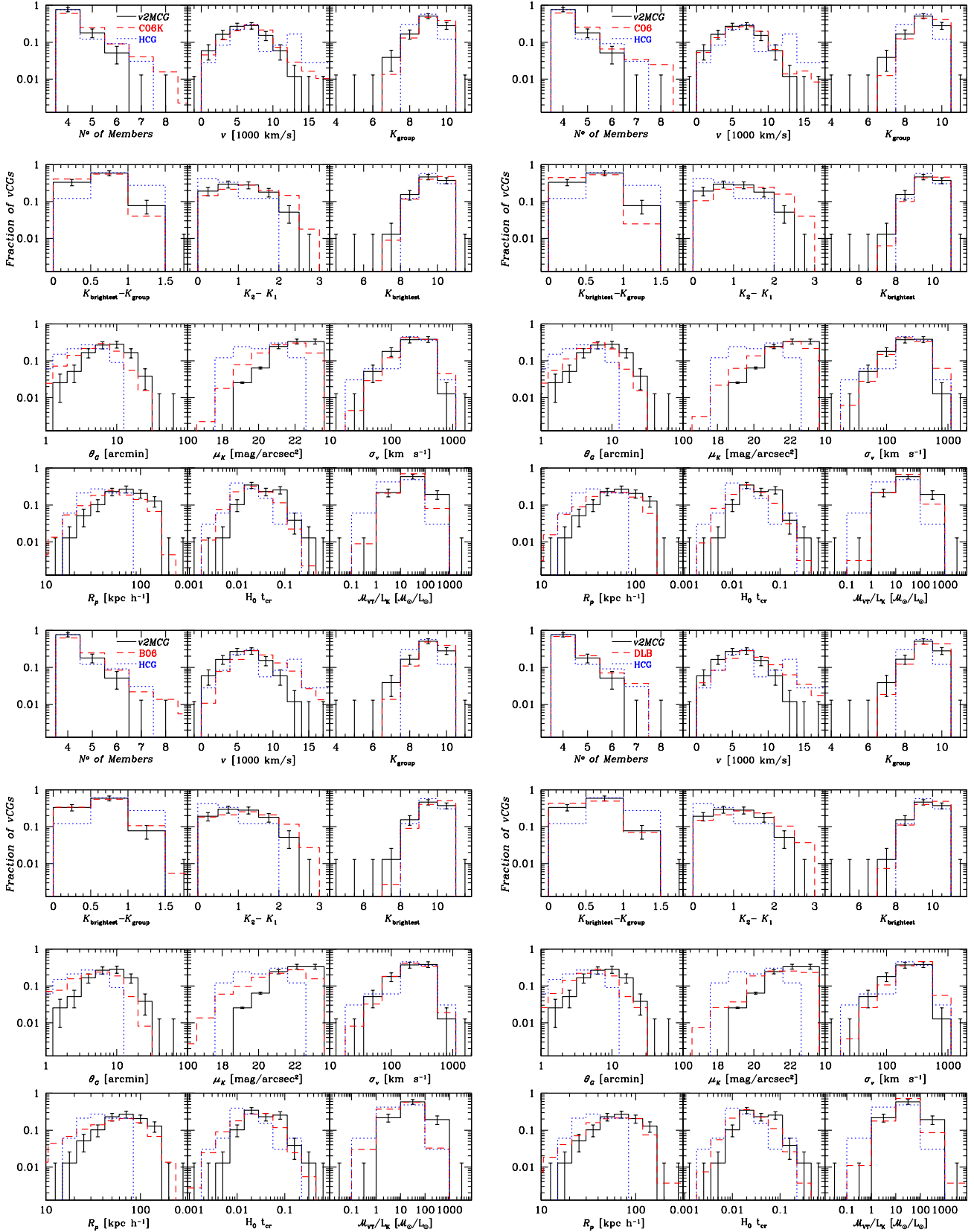


Figure B1. Distribution of properties of the *v2MCG* (solid lines) and HCG92/2 (dotted lines) samples, compared with different semi-analytical models (dashed lines). Error bars correspond to Poisson errors.

Table C1. CGs after velocity filtering in the 2MASS XSC

ID	RA (J2000)	Dec	v [km s ⁻¹]	N	K_b	μ_K [$\frac{\text{mag}}{\text{arcsec}^2}$]	θ_G [arcmin]	$\langle R_{ij} \rangle$ [kpc/h]	b/a	σ_v [km s ⁻¹]	$H_0 t_{cr}$	M_{VT}/L_K [$h M_\odot/L_\odot$]	cross-ID
1	00:00:43	28:23:18	8705	5	10.41	19.92	2.34	43.44	0.67	322	0.012	28	HCG 99, KTG 83, VV 854
2	00:00:59	-43:22:47	11525	4	10.14	22.23	6.07	121.73	0.30	479	0.023	148	...
3	00:28:54	02:45:34	4241	5	8.58	23.18	18.04	50.06	0.08	175	0.026	11	UZC-CG 7, VV 894
4	00:39:24	00:52:28	4209	4	9.33	21.00	5.58	45.56	0.53	130	0.032	10	HCG 7, UZC-CG 9, USGC U024
5	00:56:42	-52:56:40	7561	4	9.50	21.29	5.71	92.15	0.37	534	0.016	108	...
6	00:57:48	-05:02:22	5345	6	10.20	22.81	11.38	85.80	0.46	294	0.026	90	...
7	01:08:58	-45:48:11	7598	4	9.87	21.05	4.18	44.85	0.11	291	0.014	29	...
8	01:13:55	-31:48:02	5687	4	8.79	21.15	7.30	85.77	0.78	293	0.027	39	SCG 1
9	01:26:05	34:41:39	4742	4	9.21	22.08	10.63	92.15	0.41	257	0.032	44	HCG 10, RSCG 12
10	01:43:24	-34:14:40	3786	4	10.11	23.20	11.09	62.52	0.24	149	0.038	46	SCG 0141-3429
11	02:07:39	02:08:30	7042	4	10.40	22.57	7.60	89.13	0.40	443	0.018	226	HCG 15
12	02:09:49	-10:13:37	3874	5	9.04	22.82	17.94	63.75	0.12	147	0.039	10	HCG 16, USGC S077, RSCG 19, VV 1007
13	02:36:55	07:22:28	6310	4	9.48	23.38	14.37	168.32	0.50	325	0.047	110	USGC U136
14	02:42:05	-15:04:36	7437	4	10.57	21.03	3.59	53.33	0.29	73	0.066	3	SCG 19, USGC S093
15	02:45:07	-17:42:28	7412	4	9.75	22.91	13.61	164.29	0.28	218	0.068	38	HCG 21
16	03:03:50	-12:02:25	3648	4	8.73	21.52	8.45	67.71	0.32	396	0.016	122	SCG 3
17	03:07:05	-09:35:15	4851	4	9.87	21.75	7.04	65.73	0.69	330	0.018	106	HCG 23, SCG 11
18	03:07:29	-66:48:22	5580	4	9.55	23.48	16.76	194.28	0.74	174	0.101	61	SCG 0306-6659
19	03:17:44	-10:19:56	8882	4	10.06	22.58	6.97	103.54	0.35	440	0.021	135	...
20	03:20:40	-01:04:18	6288	4	10.52	21.87	4.55	47.93	0.40	87	0.050	6	HCG 25
21	03:25:22	-06:09:30	10335	4	10.44	22.12	5.85	116.75	0.36	157	0.067	17	...
22	03:46:31	-04:12:39	3917	5	8.18	23.38	29.15	140.46	0.40	145	0.088	15	...
23	04:51:45	-03:52:38	4633	4	10.14	22.83	8.34	74.54	0.57	83	0.082	13	...
24	04:59:25	-11:08:00	3823	6	9.03	22.60	18.32	99.91	0.56	357	0.025	59	KTS 28, VV 699
25	06:03:55	-32:06:38	9565	4	10.09	23.16	9.23	129.26	0.10	460	0.026	73	...
26	06:43:41	-74:14:45	6458	4	9.54	21.37	6.09	59.98	0.23	377	0.014	58	VV 785
27	07:04:34	64:03:45	4468	4	9.55	22.99	11.27	94.36	0.25	66	0.129	8	...
28	07:26:32	85:37:41	2177	4	7.74	22.71	22.30	83.25	0.46	262	0.029	98	VV 1189
29	07:40:56	55:25:55	10752	4	9.90	19.38	1.73	32.21	0.42	436	0.007	32	...
30	09:05:05	18:21:41	4188	5	9.01	23.51	17.54	142.04	0.79	391	0.033	317	VV 612
31	09:16:30	30:52:02	6954	4	9.82	22.64	8.38	85.16	0.11	73	0.106	3	...
32	09:27:57	30:00:35	7994	4	10.24	21.21	3.56	48.52	0.64	387	0.011	106	...
33	09:34:23	10:09:24	3141	4	8.86	23.29	19.19	105.31	0.37	355	0.027	207	RSCG 33, VV 1290/1292
34	09:38:55	-04:51:05	6633	5	9.73	18.60	1.74	15.19	0.36	189	0.007	4	HCG 40, VV 116
35	10:00:01	-19:34:37	4020	4	8.18	22.74	18.18	105.27	0.08	119	0.081	6	HCG 42
36	10:25:07	28:03:09	6361	4	10.14	21.84	5.07	72.55	0.84	188	0.035	47	...
37	10:37:15	-26:14:56	3433	4	9.29	22.59	10.66	79.84	0.59	268	0.027	142	...
38	10:39:43	-23:49:47	3758	4	9.97	23.32	11.88	100.45	0.95	159	0.057	71	...
39	10:51:52	50:56:02	7491	5	10.08	23.14	11.22	139.23	0.46	497	0.025	78	VV 1393
40	11:09:46	21:46:22	9552	4	10.01	21.52	4.81	64.52	0.08	103	0.057	3	...
41	11:16:12	18:07:46	896	4	7.11	21.95	21.98	36.44	0.33	289	0.011	98	...
42	11:22:21	24:18:31	7619	4	10.07	21.12	4.07	63.83	0.20	322	0.018	46	HCG 51, UZC-CG 138, VV 1435
43	11:35:11	51:12:03	8010	4	10.41	21.94	4.76	57.86	0.44	325	0.016	102	...
44	11:42:10	10:18:52	6218	5	9.63	21.86	8.82	91.33	0.60	173	0.048	17	HCG 58, UZC-CG 144
45	11:42:51	26:31:54	9054	4	10.06	22.87	9.91	126.33	0.11	355	0.032	68	...
46	11:44:06	33:30:45	9381	4	10.16	21.25	3.78	67.96	0.43	144	0.043	8	...
47	11:57:06	55:17:50	948	4	7.42	22.44	23.41	51.99	0.45	211	0.022	88	...
48	12:19:22	05:57:42	2156	4	7.40	21.67	16.44	73.71	0.39	348	0.019	89	...
49	12:24:31	07:09:38	994	5	6.79	22.83	36.02	64.63	0.46	215	0.027	91	...
50	12:27:47	12:11:30	1024	4	8.99	23.12	15.53	28.03	0.32	557	0.005	1560	...
51	12:43:17	11:25:08	1117	5	5.81	22.16	45.77	75.83	0.38	363	0.019	56	M60 CG, VV 206/1558
52	13:01:58	27:37:34	7473	4	10.03	21.90	5.07	61.27	0.21	704	0.008	401	...
53	13:06:50	-40:22:49	4768	4	8.83	22.20	10.29	118.12	0.55	116	0.092	14	HDCE 0761
54	13:08:15	34:01:53	10120	4	10.50	23.41	10.77	180.87	0.54	185	0.089	47	...
55	13:22:02	-17:21:16	6909	5	9.95	22.11	6.15	71.02	0.44	241	0.027	50	...
56	13:24:31	14:01:36	7087	4	9.37	22.75	11.94	177.44	0.47	278	0.058	76	...
57	13:52:16	02:20:05	7095	4	9.80	20.74	3.42	51.30	0.52	50	0.094	1	...
58	13:53:01	-28:27:48	4713	5	8.54	21.08	7.27	43.75	0.13	261	0.015	20	...
59	14:00:33	-02:51:35	7325	6	9.82	21.73	6.12	60.26	0.31	322	0.017	37	...
60	14:19:14	35:08:15	8534	4	10.34	22.52	6.12	74.71	0.28	52	0.131	3	...
61	14:27:27	11:19:18	8078	4	10.45	22.51	6.47	108.69	0.70	424	0.023	245	...
62	14:28:02	25:53:33	4388	4	9.33	21.86	8.31	67.15	0.58	216	0.028	42	...
63	14:58:09	-19:10:04	3387	4	8.48	23.41	23.18	158.56	0.52	107	0.134	14	...

Table C1 – *continued* — CGs after velocity filtering in the 2MASS XSC

ID	RA (J2000)	Dec	v [km s ⁻¹]	N	K_b	μ_K [$\frac{\text{mag}}{\text{arcsec}^2}$]	θ_G [arcmin]	$\langle R_{ij} \rangle$ [kpc/h]	b/a	σ_v [km s ⁻¹]	$H_0 t_{\text{cr}}$	M_{VT}/L_K [$h M_\odot/L_\odot$]	cross-ID
64	15:36:22	43:29:29	5660	5	9.62	22.19	9.19	102.35	0.71	197	0.047	28	...
65	16:12:50	33:02:06	9429	4	10.51	21.73	4.32	91.69	0.20	108	0.077	4	VV 1801
66	16:37:53	36:03:18	9614	4	9.91	22.45	7.62	105.18	0.17	204	0.047	23	...
67	19:14:47	-54:36:26	5400	4	9.48	23.15	13.64	110.24	0.13	224	0.045	33	...
68	19:51:59	-30:49:31	5891	4	9.47	20.22	3.90	46.60	0.80	368	0.011	50	HCG 86
69	20:00:59	-47:04:38	6804	4	10.02	20.19	2.92	29.28	0.16	317	0.008	30	KTS 61, Rose 38, NGC6845, VV 1880
70	20:03:14	-56:00:10	4413	4	8.01	21.62	12.97	93.18	0.30	84	0.100	3	...
71	20:17:25	-70:41:58	3969	4	7.77	22.94	28.03	167.79	0.20	488	0.031	148	VV 297
72	20:43:41	-26:34:43	12406	4	10.45	21.45	3.81	95.20	0.68	268	0.032	38	...
73	20:47:22	00:23:32	3779	6	8.89	21.83	11.03	71.64	0.58	254	0.026	43	...
74	20:52:24	-05:45:16	6028	4	9.85	22.19	7.70	68.51	0.16	80	0.077	5	HCG 88
75	21:08:25	-29:45:32	5935	4	9.57	23.48	14.46	166.54	0.82	53	0.285	6	SCG 2105-2957
76	21:17:01	-42:19:38	5337	4	9.46	22.32	9.77	123.47	0.81	112	0.100	11	SCG 2113-4235
77	22:03:28	12:38:56	8113	4	9.83	20.15	2.66	39.48	0.51	465	0.008	69	WBL 677
78	22:36:24	-24:18:35	10314	4	10.30	21.57	4.21	95.89	0.12	103	0.084	4	...
79	22:55:22	-33:54:22	8761	4	10.21	20.21	2.39	41.13	0.65	175	0.021	10	VV 1957
80	22:58:09	26:07:30	7588	5	9.25	22.17	8.95	137.84	0.72	201	0.062	22	UZC-CG 282, VV 84
81	23:15:18	19:00:38	4922	4	9.00	21.58	8.31	70.59	0.41	237	0.027	37	HCG 93, USGC U837, Arp 99
82	23:28:03	-67:47:18	3904	4	9.82	21.54	6.04	42.88	0.46	176	0.022	25	...
83	23:28:18	32:25:09	5066	4	9.18	21.58	7.15	68.01	0.59	344	0.018	58	...
84	23:47:27	-02:18:37	6665	5	10.07	21.38	5.23	64.89	0.73	415	0.014	94	HCG 97, RSCG 87
85	23:53:35	07:59:10	5218	5	9.15	22.68	15.93	142.35	0.52	233	0.055	33	...

Notes. ID: Group ID, RA: Right Ascension of the CG centre, Dec: Declination of the CG centre, v : Median velocity, N : Number of galaxy members in the CG in the range of 3 magnitudes from the brightest member, K_b : Galactic Extinction-corrected K -band apparent magnitude of the brightest galaxy, μ_K : Galactic Extinction-corrected K -band group surface brightness, θ_G : Angular diameter of the smallest circumscribed circle, $\langle R_{ij} \rangle$: Median projected separation among galaxies, b/a : Apparent group elongation, σ_v : Radial velocity dispersion of the galaxies in the CG computed using individual galaxy errors, $H_0 t_{\text{cr}}$: Dimensionless crossing time, M_{VT}/L_K : Mass to Light ratio in the K -band, cross-ID: Cross-identification with other group catalogues

References for cross-ID: AM: Arp+Madore Southern Peculiar Galaxies and Associations (Arp & Madore 1987); Arp: Arp Peculiar Galaxies (Arp 1966); HCG: Hickson Compact Group (Hickson 1982); HDCE: High-density-contrast groups - Erratum version (Crook et al. 2008); KPG: Karachentsev Isolated Pairs of Galaxies Catalogue (Karachentsev 1972); KTG: Karachentsev Isolated Triplets of Galaxies Catalogue (Karachentsev et al. 1988); KTS: Karachentseva Triple System (Karachentseva & Karachentsev 2000); M60: (Mamon 1989, 2008); Rose: Rose Compact Groups of Galaxies (Rose 1977); RSCG: Redshift Survey Compact Group (Barton et al. 1996); SCG: Southern Compact Group (Prandoni et al. 1994; Iovino 2002); UZC-CG: Updated Zwicky Catalogue-Compact Group (Focardi & Kelm 2002); USGC: UZC/SSRS2 Group Catalogue (Ramella et al. 2002); VV: Interacting galaxies catalogue (Vorontsov-Velyaminov et al. 2001) WBL: White+Bliton+Bhavsar groups (White et al. 1999);

Table C2. Table of galaxy members (*v*2MCGs)

GroupID	GalID	RA	Dec	K	k_K	v	$\text{err}(v)$	v	SDSS_ID	2MASS_ID
		(J2000)				[km s^{-1}]		source		
1	1	00:00:46.97	28:24:07.28	10.41	-0.06	8764	19	1	758874298530726152	00004696+2824071
1	2	00:00:37.94	28:23:04.34	10.46	-0.05	8705	9	1	758874298530726255	00003794+2823041
1	3	00:00:44.00	28:24:05.22	11.53	-0.04	8156	0	1	758874298530726153	00004401+2824051
1	4	00:00:42.41	28:22:08.43	13.26	-0.03	9006	0	2	758874298530791466	00004242+2822081
1	5	00:00:45.09	28:22:18.18	13.40	-0.08	8642	0	2	758874298530791773	00004507+2822181
2	1	00:01:02.89	-43:19:49.57	10.14	-0.07	11627	45	1	000000000000000000	00010289-4319496
2	2	00:00:53.00	-43:23:31.43	11.59	-0.05	11980	40	1	000000000000000000	00005298-4323316
2	3	00:00:57.05	-43:25:47.60	12.27	-0.06	10964	45	2	000000000000000000	00005702-4325476
2	4	00:00:52.18	-43:20:02.38	12.47	-0.06	11422	0	2	000000000000000000	00005216-4320026
3	1	00:29:15.06	02:51:50.58	8.58	-0.02	4241	16	1	000000000000000000	00291506+0251505
3	2	00:28:29.78	02:38:54.98	10.88	-0.03	4317	29	1	000000000000000000	00282976+0238549
3	3	00:29:08.10	02:48:39.97	11.36	-0.03	4046	25	1	000000000000000000	00290809+0248400
3	4	00:29:18.55	02:52:13.56	11.51	-0.03	4433	0	1	000000000000000000	00291854+0252135
3	5	00:29:12.40	02:52:21.42	11.53	-0.02	4093	0	1	000000000000000000	00291239+0252215
4	1	00:39:13.39	00:51:50.87	9.33	-0.03	4177	3	1	588015510347382842	00391339+0051508
4	2	00:39:17.84	00:54:45.88	10.14	-0.03	4239	1	1	588015510347382865	00391786+0054458
4	3	00:39:34.85	00:51:35.68	10.51	-0.03	4379	3	1	588015510347448339	00393485+0051355
4	4	00:39:18.79	00:53:31.01	12.07	-0.02	4107	0	2	588015510347382868	00391879+0053308
5	1	00:56:41.65	-52:58:33.32	9.50	-0.05	7779	31	1	000000000000000000	00564165-5258332
5	2	00:56:57.57	-52:55:26.10	10.08	-0.04	7342	29	1	000000000000000000	00565758-5255262
5	3	00:56:43.64	-52:53:49.16	11.85	-0.04	7331	28	2	000000000000000000	00564365-5253492
5	4	00:56:42.17	-52:59:31.44	12.29	-0.06	8392	45	2	000000000000000000	00564220-5259312
6	1	00:58:01.60	-05:04:16.44	10.20	-0.03	5184	45	1	000000000000000000	00580158-0504165
6	2	00:57:55.36	-05:07:49.53	10.34	-0.03	5314	45	1	000000000000000000	00575536-0507495
6	3	00:57:42.39	-04:56:55.11	10.96	-0.03	5375	45	1	000000000000000000	00574239-0456548
6	4	00:57:47.87	-05:06:43.52	11.16	-0.03	5454	36	1	000000000000000000	00574786-0506435
6	5	00:57:39.24	-05:05:09.92	11.60	-0.03	4845	45	1	000000000000000000	00573925-0505098
6	6	00:57:35.09	-05:00:09.00	11.73	-0.04	5675	45	1	000000000000000000	00573510-0500088
7	1	01:09:04.55	-45:46:24.73	9.87	-0.05	7746	27	1	000000000000000000	01090456-4546246
7	2	01:08:51.85	-45:49:57.50	10.60	-0.05	7207	37	1	000000000000000000	01085185-4549577
7	3	01:08:57.40	-45:48:15.63	12.60	-0.05	7768	0	2	000000000000000000	01085740-4548157
7	4	01:09:01.03	-45:48:04.83	12.86	-0.07	7449	0	2	000000000000000000	01090103-4548047
8	1	01:13:47.26	-31:44:50.00	8.79	-0.04	5738	45	1	000000000000000000	01134725-3144500
8	2	01:13:51.26	-31:47:18.04	9.62	-0.04	5636	19	1	000000000000000000	01135125-3147180
8	3	01:14:10.95	-31:49:38.06	10.89	-0.04	5594	45	1	000000000000000000	01141094-3149382
8	4	01:13:43.18	-31:50:35.21	11.25	-0.05	6228	45	1	000000000000000000	01134317-3150350
9	1	01:25:40.29	34:42:46.68	9.21	-0.04	4822	18	1	758877278694080872	01254030+3442465
9	2	01:26:21.78	34:42:10.89	9.34	-0.03	5188	5	1	758877153601913092	01262177+3442107
9	3	01:26:18.83	34:45:14.93	10.62	-0.03	4660	32	1	758877153601978381	01261884+3445147
9	4	01:26:30.85	34:40:31.76	11.64	-0.02	4662	0	1	758877153601913329	01263085+3440318
10	1	01:43:09.68	-34:14:30.85	10.11	-0.03	3801	45	1	000000000000000000	01430966-3414305
10	2	01:43:18.35	-34:12:21.62	10.72	-0.01	3770	45	1	000000000000000000	01431837-3412216
10	3	01:43:45.06	-34:18:07.33	11.30	-0.03	3756	31	1	000000000000000000	01434505-3418070
10	4	01:43:02.96	-34:11:14.44	12.47	-0.02	4093	32	2	000000000000000000	01430297-3411143
11	1	02:07:53.08	02:10:03.37	10.40	-0.05	6966	30	1	000000000000000000	02075306+0210034
11	2	02:07:34.13	02:06:55.17	11.01	-0.05	7117	36	1	000000000000000000	02073411+0206554
11	3	02:07:37.52	02:10:50.62	11.50	-0.04	6243	36	1	000000000000000000	02073751+0210504
11	4	02:07:25.29	02:06:58.08	11.76	-0.05	7196	0	2	000000000000000000	02072527+0206579
12	1	02:09:24.60	-10:08:09.15	9.04	-0.02	4174	45	1	587727177926508587	02092458-1008091
12	2	02:09:20.86	-10:07:59.15	9.54	-0.02	3854	2	1	587727177926508588	02092086-1007591
12	3	02:09:38.53	-10:08:46.57	9.81	-0.01	3849	1	1	587727177926574089	02093853-1008466
12	4	02:09:42.74	-10:11:01.80	9.92	-0.01	3874	5	1	000000000000000000	02094273-1011016
12	5	02:10:17.55	-10:19:15.72	10.61	-0.02	4045	45	1	000000000000000000	02101756-1019157
13	1	02:37:14.48	07:18:20.27	9.48	-0.04	6498	61	1	587744296044986466	02371447+0718201
13	2	02:36:31.62	07:18:34.23	10.77	-0.02	6122	3	1	587744296044920962	02363162+0718342
13	3	02:37:16.50	07:20:08.95	11.46	-0.05	6546	49	1	587744296044986609	02371649+0720091
13	4	02:37:20.26	07:26:23.32	11.52	-0.03	5931	0	1	587744296044986628	02375206+0726231
14	1	02:42:06.28	-15:05:29.24	10.57	-0.05	7396	31	1	000000000000000000	02420629-1505289
14	2	02:42:05.74	-15:02:48.78	10.58	-0.04	7328	23	1	000000000000000000	02420573-1502489
14	3	02:42:04.98	-15:06:23.88	12.03	-0.05	7477	270	3	000000000000000000	02420497-1506239
14	4	02:42:01.38	-15:03:23.91	12.74	-0.06	7476	0	2	000000000000000000	02420138-1503239

Table C2 – *continued* — Table of galaxy positions

GroupID	GalID	RA	Dec	K	k_K	v	err(v)	v	SDSS_ID	2MASS_ID
		(J2000)				[km s ⁻¹]		source		
15	1	02:44:53.65	-17:39:32.92	9.75	-0.05	7272	45	1	000000000000000000	02445363-1739330
15	2	02:45:36.08	-17:41:20.16	9.83	-0.04	7550	45	1	000000000000000000	02453607-1741201
15	3	02:45:18.02	-17:42:30.09	9.99	-0.04	7682	45	1	000000000000000000	02451802-1742301
15	4	02:44:39.73	-17:43:35.99	12.01	-0.05	7272	45	2	000000000000000000	02443974-1743359
16	1	03:03:54.48	-11:59:30.48	8.73	-0.03	3986	45	1	000000000000000000	03035448-1159306
16	2	03:03:35.20	-12:04:34.72	9.94	-0.03	3384	22	1	000000000000000000	03033518-1204349
16	3	03:04:06.22	-12:00:55.65	11.13	-0.02	3265	35	1	000000000000000000	03040620-1200556
16	4	03:03:32.80	-12:02:23.16	11.17	-0.03	3911	36	1	000000000000000000	03033280-1202229
17	1	03:06:55.94	-09:32:38.66	9.87	-0.03	4825	45	1	000000000000000000	03065595-0932389
17	2	03:07:09.47	-09:35:33.55	10.11	-0.02	4876	11	1	000000000000000000	03070944-0935334
17	3	03:07:18.38	-09:36:45.48	10.56	-0.03	5199	45	1	000000000000000000	03071837-0936454
17	4	03:06:55.22	-09:37:42.86	12.00	-0.04	4466	21	2	000000000000000000	03065521-0937429
18	1	03:06:31.08	-66:46:32.20	9.55	-0.03	5521	10	1	000000000000000000	03063104-6646320
18	2	03:07:02.09	-66:56:19.20	9.99	-0.04	5639	45	1	000000000000000000	03070209-6656192
18	3	03:07:40.74	-66:40:04.47	10.92	-0.04	5762	45	1	000000000000000000	03074073-6640045
18	4	03:08:39.99	-66:53:03.40	11.44	-0.04	5398	45	1	000000000000000000	03083999-6653035
19	1	03:17:45.52	-10:17:20.72	10.06	-0.06	8984	39	1	000000000000000000	03174554-1017207
19	2	03:17:35.93	-10:18:50.78	11.94	-0.05	8778	45	2	000000000000000000	03173593-1018511
19	3	03:17:42.95	-10:23:24.41	12.61	-0.05	9562	0	2	000000000000000000	03174295-1023247
19	4	03:17:46.00	-10:16:28.59	12.82	-0.06	8633	0	2	000000000000000000	03174601-1016287
20	1	03:20:45.41	-01:02:40.87	10.52	-0.04	6413	3	1	587731511545757880	03204541-0102407
20	2	03:20:42.94	-01:06:30.89	11.66	-0.03	6268	2	1	588015507680723132	03204294-0106307
20	3	03:20:38.55	-01:02:06.05	12.41	-0.05	6307	2	2	587731511545757775	03203854-0102057
20	4	03:20:45.34	-01:03:14.06	12.51	-0.03	6229	0	2	588015507680723008	03204534-0103137
21	1	03:25:11.58	-06:10:51.17	10.44	-0.05	10092	2	1	587724242304565362	03251157-0610510
21	2	03:25:25.37	-06:08:38.02	10.82	-0.05	10316	3	1	587724242304630856	03252538-0608380
21	3	03:25:31.39	-06:07:43.98	11.93	-0.05	10435	2	2	587724242304630877	03253137-0607438
21	4	03:25:19.37	-06:12:21.02	13.01	-0.04	10353	0	2	587724242304630917	03251935-0612210
22	1	03:46:27.25	-03:58:07.63	8.18	-0.02	3908	45	1	000000000000000000	03462726-0358075
22	2	03:45:43.12	-04:05:29.68	9.27	-0.02	3972	45	1	000000000000000000	03454312-0405295
22	3	03:46:35.94	-04:27:11.52	9.62	-0.02	3740	45	1	000000000000000000	03463595-0427115
22	4	03:46:07.16	-04:04:09.13	9.98	-0.03	3916	45	1	000000000000000000	03460717-0404093
22	5	03:46:03.07	-04:08:17.17	10.07	-0.03	4136	45	1	000000000000000000	03460309-0408173
23	1	04:51:41.51	-03:48:33.68	10.14	-0.02	4764	30	1	758885351078232088	04514150-0348335
23	2	04:51:55.95	-03:55:47.66	11.48	-0.03	4607	23	1	758887369173827734	04515593-0355475
23	3	04:51:41.75	-03:50:29.54	11.95	-0.03	4578	45	2	758885351078232404	04514177-0350295
23	4	04:51:28.41	-03:52:12.53	12.09	-0.02	4659	45	2	758885351078166820	04512841-0352124
24	1	04:59:25.89	-10:58:50.54	9.03	-0.03	3740	7	1	000000000000000000	04592589-1058504
24	2	04:59:27.73	-11:07:22.62	9.24	-0.02	3762	11	1	000000000000000000	04592771-1107224
24	3	04:59:17.38	-11:07:07.20	9.35	-0.03	4500	9	1	000000000000000000	04591738-1107071
24	4	04:59:22.89	-11:07:56.34	9.43	-0.02	3883	42	1	000000000000000000	04592288-1107561
24	5	04:59:41.37	-11:16:17.44	10.77	-0.02	3700	45	1	000000000000000000	04594137-1116175
24	6	04:58:50.32	-11:04:53.04	11.78	-0.02	4390	45	2	000000000000000000	04585029-1104531
25	1	06:03:39.89	-32:08:52.03	10.09	-0.05	9233	38	1	000000000000000000	06033989-3208521
25	2	06:03:38.22	-32:09:19.99	11.96	-0.06	9912	45	2	000000000000000000	06033824-3209201
25	3	06:04:13.62	-32:03:57.30	12.33	-0.03	9090	45	2	000000000000000000	06041362-3203574
25	4	06:03:42.26	-32:09:42.48	12.41	-0.04	9896	45	2	000000000000000000	06034225-3209422
26	1	06:43:06.02	-74:14:10.45	9.54	-0.04	6504	120	1	000000000000000000	06430596-7414103
26	2	06:44:17.48	-74:16:36.32	10.61	-0.04	6153	28	1	000000000000000000	06441744-7416364
26	3	06:43:25.51	-74:15:25.74	10.64	-0.04	6411	33	1	000000000000000000	06432557-7415255
26	4	06:43:06.00	-74:12:55.17	11.21	-0.05	7000	150	1	000000000000000000	06430602-7412553
27	1	07:04:20.30	64:01:12.98	9.55	-0.03	4497	6	1	000000000000000000	07042030+6401132
27	2	07:05:23.68	64:05:32.50	11.33	-0.02	4530	48	1	000000000000000000	07052368+6405326
27	3	07:03:45.99	64:01:57.06	11.50	-0.03	4380	0	1	000000000000000000	07034600+6401570
27	4	07:05:19.69	64:02:26.83	11.54	-0.04	4438	0	1	000000000000000000	07051971+6402266
28	1	07:32:20.49	85:42:31.90	7.74	-0.01	1905	7	1	000000000000000000	07322048+8542319
28	2	07:27:14.36	85:45:16.37	9.25	-0.01	2415	2	1	000000000000000000	07271448+8545162
28	3	07:34:57.53	85:32:13.90	10.03	-0.02	2050	51	1	000000000000000000	07345760+8532138
28	4	07:17:47.09	85:42:47.75	10.61	-0.02	2303	22	1	000000000000000000	07174680+8542479
29	1	07:40:58.22	55:25:37.92	9.90	-0.06	10229	27	1	000000000000000000	07405822+5525379
29	2	07:41:00.08	55:25:13.89	11.84	-0.03	11037	0	2	000000000000000000	07410010+5525139
29	3	07:40:52.73	55:26:36.89	12.20	-0.06	11018	0	2	000000000000000000	07405269+5526369
29	4	07:40:59.74	55:26:21.01	12.66	-0.07	10485	0	2	000000000000000000	07405974+5526209

Table C2 – continued — Table of galaxy positions

GroupID	GalID	RA	Dec	K	k_K	v	err(v)	v	SDSS_ID	2MASS_ID
		(J2000)				[km s ⁻¹]		source		
30	1	09:05:21.32	18:18:47.18	9.01	-0.03	4189	21	1	587741708330074118	09052131+1818472
30	2	09:04:39.02	18:27:51.92	11.08	-0.02	3423	5	1	587741708330008623	09043901+1827521
30	3	09:05:32.39	18:15:44.45	11.45	-0.04	4250	2	1	588023045866193011	09053239+1815445
30	4	09:04:39.32	18:15:26.33	11.94	-0.03	3635	2	2	587741708329943218	09043929+1815261
30	5	09:05:18.35	18:26:32.15	11.95	-0.03	4188	2	2	587741708330074178	09051836+1826322
31	1	09:16:41.85	30:54:55.33	9.82	-0.04	6949	2	1	588017979413299278	09164185+3054551
31	2	09:16:15.64	30:49:26.32	11.60	-0.05	6812	2	1	588017979413233753	09161561+3049261
31	3	09:16:37.66	30:54:19.33	11.65	-0.05	6958	2	1	588017979413299279	09163765+3054191
31	4	09:16:46.19	30:54:39.25	12.32	-0.02	6974	2	2	588017979413299280	09164620+3054391
32	1	09:27:52.82	29:59:08.64	10.24	-0.04	7993	2	1	587739158725001301	09275281+2959085
32	2	09:28:00.92	30:02:13.33	11.81	-0.06	7993	2	2	587739158725001338	09280090+3002135
32	3	09:28:04.06	29:59:29.31	12.30	-0.05	8296	1	2	587739115781947490	09280405+2959294
32	4	09:27:57.72	30:00:39.63	12.97	-0.01	7424	0	2	587739158725001442	09275774+3000395
33	1	09:33:46.09	10:09:09.09	8.86	-0.02	3231	2	3	587735344799350868	09334609+1009093
33	2	09:34:02.78	10:06:31.49	9.99	-0.02	3144	1	1	587735344799350940	09340276+1006315
33	3	09:34:47.54	10:17:01.42	10.15	-0.01	2432	8	1	587735344799481904	09344754+1017014
33	4	09:34:00.18	10:01:46.51	11.37	-0.02	3136	5	1	587734949661769909	09340019+1001465
34	1	09:38:53.47	-04:50:55.32	9.73	-0.05	6627	27	1	000000000000000000	09385347-0450553
34	2	09:38:53.62	-04:51:36.58	10.32	-0.03	6405	6	1	000000000000000000	09385360-0451365
34	3	09:38:54.96	-04:51:57.31	10.71	-0.05	6842	27	1	000000000000000000	09385496-0451573
34	4	09:38:55.76	-04:50:13.45	10.92	-0.04	6837	45	1	000000000000000000	09385576-0450134
34	5	09:38:55.29	-04:51:28.47	12.17	-0.04	6632	23	2	000000000000000000	09385529-0451284
35	1	10:00:14.14	-19:38:11.21	8.18	-0.03	3964	10	1	000000000000000000	10001412-1938113
35	2	09:59:29.19	-19:29:32.18	10.12	-0.03	4004	17	1	000000000000000000	09592917-1929323
35	3	10:00:10.29	-19:37:18.53	10.40	-0.03	4034	45	1	000000000000000000	10001030-1937183
35	4	10:00:33.11	-19:39:43.13	10.63	-0.03	4228	18	1	000000000000000000	10003309-1939433
36	1	10:24:59.32	28:01:26.00	10.14	-0.05	6417	27	1	587741566050304065	10245932+2801259
36	2	10:25:07.28	28:05:41.04	11.60	-0.04	6130	2	1	587741566050369539	10250725+2805409
36	3	10:25:13.58	28:00:58.31	12.26	-0.04	6520	2	2	587741534390517974	10251359+2800584
36	4	10:25:18.72	28:03:20.38	12.43	-0.04	6304	0	2	587741566050369557	10251872+2803204
37	1	10:37:29.09	-26:19:01.22	9.29	-0.02	3358	45	1	000000000000000000	10372908-2619014
37	2	10:36:56.64	-26:11:39.32	10.88	-0.02	3251	45	1	000000000000000000	10365664-2611391
37	3	10:37:37.87	-26:16:38.32	10.97	-0.02	3815	45	1	000000000000000000	10373785-2616384
37	4	10:37:00.43	-26:19:05.25	11.78	-0.02	3507	45	2	000000000000000000	10370041-2619051
38	1	10:39:34.06	-23:55:21.69	9.97	-0.03	3813	45	1	000000000000000000	10393405-2355217
38	2	10:40:08.94	-23:49:13.31	10.69	-0.03	3619	45	1	000000000000000000	10400892-2349132
38	3	10:39:26.11	-23:45:17.50	11.56	-0.01	3955	45	1	000000000000000000	10392612-2345176
38	4	10:39:40.26	-23:53:15.73	12.83	-0.02	3703	0	2	000000000000000000	10394025-2353157
39	1	10:51:43.67	51:01:19.76	10.08	-0.05	7491	3	1	588013383811923987	10514368+5101195
39	2	10:51:44.49	51:01:30.32	10.44	-0.04	7137	0	1	588013383811923988	10514450+5101303
39	3	10:51:53.71	51:00:23.47	12.01	-0.05	8277	3	2	588013383811924105	10515373+5100234
39	4	10:51:23.23	50:55:51.54	12.24	-0.03	7281	2	2	588013383811858538	10512323+5055516
39	5	10:52:00.77	50:50:34.70	12.55	-0.05	7805	0	2	588013383811924012	10520073+5050344
40	1	11:09:44.43	21:45:31.88	10.01	-0.06	9542	2	1	587742061602734111	11094441+2145316
40	2	11:09:50.31	21:48:36.88	11.40	-0.06	9432	2	1	587742014350557248	11095029+2148366
40	3	11:09:41.19	21:44:25.54	11.62	-0.05	9659	2	1	587742061602734109	11094118+2144256
40	4	11:09:42.82	21:44:07.82	12.37	-0.07	9562	0	0	587742061602734112	11094283+2144076
41	1	11:16:54.66	18:03:06.51	7.11	-0.01	959	20	1	587742865818779699	11165465+1803065
41	2	11:16:58.95	18:08:54.95	8.17	-0.01	1253	5	1	587742571074355242	11165896+1808547
41	3	11:15:26.95	18:06:37.29	9.48	-0.01	832	9	1	587742571074158634	11152695+1806373
41	4	11:16:46.61	18:01:01.74	9.78	-0.01	642	1	1	587742865818779669	11164662+1801017
42	1	11:22:26.35	24:17:56.93	10.07	-0.05	7539	2	1	587741829122555933	11222635+2417567
42	2	11:22:13.28	24:19:02.12	11.24	-0.05	7699	23	1	587742190436352010	11221325+2419017
42	3	11:22:14.22	24:18:00.88	11.47	-0.06	8200	3	1	587741829122556024	11221420+2418007
42	4	11:22:30.55	24:17:59.96	11.99	-0.06	7527	2	2	587741829122555934	11223052+2417597
43	1	11:35:00.00	51:13:04.81	10.41	-0.05	8085	2	1	588013382204194882	11345999+5113048
43	2	11:35:13.62	51:09:42.87	11.75	-0.05	7949	2	1	588013382204194936	11351359+5109426
43	3	11:35:15.64	51:12:13.68	12.22	-0.05	7393	2	2	588013382204194957	11351563+5112136
43	4	11:35:08.66	51:14:24.72	13.14	-0.04	8071	0	2	588013382204194911	11350862+5114247
44	1	11:42:11.09	10:16:39.88	9.63	-0.02	6267	6	1	587734893288095762	11421107+1016398
44	2	11:42:23.72	10:15:50.88	9.92	-0.04	6475	2	1	587734893288095841	11422374+1015508
44	3	11:41:52.95	10:18:15.83	10.30	-0.04	6074	2	1	587732772126261318	11415296+1018160
44	4	11:42:05.86	10:21:04.51	10.70	-0.04	6217	2	1	587732772126261358	11420585+1021047
44	5	11:42:04.90	10:23:02.98	11.81	-0.02	6093	4	2	587732772126261508	11420490+1023027

Table C2 – *continued* — Table of galaxy positions

GroupID	GalID	RA	Dec	K	k_K	v	err(v)	v	SDSS_ID	2MASS_ID
		(J2000)				[km s ⁻¹]		source		
45	1	11:42:32.86	26:29:19.89	10.06	-0.05	9090	3	1	587741600954712088	11423285+2629198
45	2	11:42:52.24	26:32:26.21	10.93	-0.05	8543	2	1	587741600954712170	11425225+2632260
45	3	11:43:11.85	26:33:32.17	11.05	-0.06	9017	3	1	587741600954777644	11431185+2633320
45	4	11:43:10.74	26:34:28.25	11.67	-0.06	9320	3	1	587741708346327131	11431073+2634280
46	1	11:44:13.99	33:30:52.21	10.16	-0.06	9517	3	1	587739405705150546	11441398+3330521
46	2	11:44:03.35	33:32:06.14	11.73	-0.05	9325	3	1	587739405705150521	11440335+3332060
46	3	11:44:09.32	33:28:56.16	12.33	-0.05	9435	3	2	587739405705150653	11440934+3328561
46	4	11:44:04.32	33:32:33.97	12.65	-0.04	9230	0	2	587739405705150522	11440431+3332340
47	1	11:57:56.15	55:27:12.79	7.42	-0.01	1040	13	1	587733081348571206	11575616+5527128
47	2	11:56:28.15	55:07:31.15	8.92	-0.01	1113	3	1	587731869633871916	11562816+5507313
47	3	11:55:45.11	55:19:14.29	9.63	-0.01	855	4	1	587733081348440213	11554511+5519144
47	4	11:57:35.58	55:27:31.64	9.63	-0.01	695	40	1	587733081348571153	11573559+5527318
48	1	12:19:23.26	05:49:28.96	7.40	-0.02	2238	7	1	588010360162091053	12192326+0549289
48	2	12:19:22.24	06:05:55.53	8.64	-0.01	1776	2	1	588010360698961934	12192224+0605556
48	3	12:25:42.66	07:13:00.33	9.98	-0.02	2507	1	1	588010880371851309	12254263+0713001
48	4	12:19:49.19	06:00:53.93	10.02	-0.02	2073	19	1	588010880371851341	12194918+0600541
49	1	12:24:28.23	07:19:03.07	6.79	-0.01	1242	6	1	588017729225752606	12242822+0719030
49	2	12:23:39.00	07:03:14.33	9.04	-0.01	751	24	1	588017728688750698	12233902+0703141
49	3	12:23:38.69	06:57:14.32	9.05	-0.01	993	1	1	588017728688750678	12233869+0657141
49	4	12:24:54.92	07:26:40.24	9.41	0.00	771	3	1	588017729225818214	12245493+0726404
49	5	12:25:42.66	07:13:00.33	9.78	-0.01	999	5	1	588017724937994262	12254263+0713001
50	1	12:27:53.57	12:17:35.62	8.99	-0.01	723	18	1	588017703470366754	12275357+1217354
50	2	12:27:27.36	12:17:25.20	10.56	-0.01	934	10	1	588017703470301335	12272735+1217252
50	3	12:27:41.22	12:18:57.41	10.95	-0.01	1113	2	1	588017703470301247	12274122+1218574
50	4	12:28:08.59	12:05:35.74	11.25	-0.02	1921	3	1	588017566027546723	12280859+1205356
51	1	12:43:40.00	11:33:09.40	5.81	-0.01	1116	6	1	588017702398328841	12434000+1133093
51	2	12:42:02.32	11:38:48.95	6.86	0.00	409	6	1	588017569774370819	12420232+1138489
51	3	12:43:32.55	11:34:56.88	8.19	-0.01	1394	5	1	588017702398263345	12433254+1134568
51	4	12:44:31.98	11:11:25.89	8.23	-0.01	1083	4	1	588017569237762053	12443197+1111259
51	5	12:42:47.43	11:26:32.89	8.24	-0.01	1164	10	1	588017702398197833	12424743+1126328
52	1	13:01:53.75	27:37:27.87	10.03	-0.06	7856	2	1	587741602573058054	13015375+2737277
52	2	13:02:07.91	27:38:54.03	12.02	-0.05	6898	2	2	587741602573058113	13020791+2738539
52	3	13:01:48.39	27:36:14.48	12.88	-0.06	8229	0	2	587741602572992587	13014841+2736147
52	4	13:02:01.05	27:39:10.80	12.90	-0.05	7089	0	2	587741602573058178	13020106+2739109
53	1	13:06:26.13	-40:24:52.56	8.83	0.00	4500	14	1	000000000000000000	13062614-4024521
53	2	13:06:32.24	-40:19:07.21	11.12	-0.03	4772	45	1	000000000000000000	13063226-4019071
53	3	13:07:16.26	-40:21:02.55	11.15	-0.04	4778	45	1	000000000000000000	13071625-4021026
53	4	13:07:12.09	-40:24:27.36	11.31	-0.03	4764	59	1	000000000000000000	13071206-4024276
54	1	13:08:35.62	33:58:33.03	10.50	-0.06	10151	3	1	587739406786560053	13083562+3358330
54	2	13:07:54.82	34:05:13.34	11.17	-0.06	10087	3	1	587739406786494548	13075483+3405131
54	3	13:08:04.17	34:00:27.19	11.26	-0.06	9943	3	1	587739406786494592	13080418+3400272
54	4	13:08:27.01	34:04:13.37	12.20	-0.03	10339	0	2	587739406786560033	13082700+3404129
55	1	13:21:50.81	-17:20:11.35	9.95	-0.05	7064	39	1	000000000000000000	13215080-1720114
55	2	13:21:54.15	-17:21:36.41	11.89	-0.05	6908	45	2	000000000000000000	13215415-1721364
55	3	13:22:07.60	-17:24:07.86	12.07	-0.02	7370	45	2	000000000000000000	13220758-1724080
55	4	13:22:15.68	-17:21:38.06	12.69	-0.03	6888	0	2	000000000000000000	13221568-1721380
55	5	13:22:06.79	-17:22:37.51	12.72	-0.05	6767	0	2	000000000000000000	13220680-1722374
56	1	13:24:10.02	13:58:35.32	9.37	-0.05	6885	2	1	587738568710357008	13241000+1358351
56	2	13:24:28.90	14:05:33.28	9.98	-0.05	7320	27	1	587736808298774638	13242889+1405332
56	3	13:24:24.17	13:56:15.19	11.51	-0.04	6826	2	1	587738568710357048	13242415+1356152
56	4	13:24:52.47	14:04:38.15	12.25	-0.03	7288	5	2	587736808298840234	13245247+1404382
57	1	13:52:10.08	02:19:30.39	9.80	-0.05	7109	31	1	587726032797696030	13521008+0219305
57	2	13:52:22.83	02:20:44.83	11.64	-0.05	6997	2	1	587726032797696100	13522284+0220448
57	3	13:52:14.56	02:21:34.31	12.05	-0.04	7107	3	2	587726032797696243	13521455+0221345
57	4	13:52:11.55	02:18:54.71	12.51	-0.04	7082	0	2	587726032797696031	13521155+0218545
58	1	13:52:53.32	-28:29:21.54	8.54	-0.03	4713	45	1	000000000000000000	13525331-2829213
58	2	13:52:59.18	-28:28:14.39	10.60	-0.03	4783	45	1	000000000000000000	13525917-2828141
58	3	13:53:15.02	-28:25:39.40	10.74	-0.03	4427	35	1	000000000000000000	13531502-2825391
58	4	13:53:00.18	-28:27:06.35	11.24	-0.03	5047	25	1	000000000000000000	13530016-2827061
58	5	13:52:48.39	-28:29:58.18	11.45	-0.03	4531	45	1	000000000000000000	13524838-2829584
59	1	14:00:37.20	-02:51:28.05	9.82	-0.04	7446	2	1	587729776905486440	14003719-0251281
59	2	14:00:30.06	-02:48:38.40	11.25	-0.05	7856	3	1	587729776905486416	14003005-0248387
59	3	14:00:36.60	-02:54:32.37	11.49	-0.04	7204	16	1	587729772610125865	14003658-0254321
59	4	14:00:37.98	-02:54:22.37	11.95	-0.05	7581	2	2	587729772610125863	14003799-0254221
59	5	14:00:37.52	-02:52:23.13	12.12	-0.04	7064	2	2	587729776905486441	14003752-0252231

Table C2 – continued — Table of galaxy positions

GroupID	GalID	RA	Dec	K	k_K	v	err(v)	v	SDSS_ID	2MASS_ID
		(J2000)				[km s ⁻¹]		source		
60	1	14:19:17.62	35:08:16.58	10.34	-0.05	8529	26	1	587736940371247137	14191759+3508168
60	2	14:19:21.31	35:05:31.69	11.86	-0.05	8459	2	2	587736940371247186	14192133+3505318
60	3	14:19:07.73	35:10:58.80	12.86	-0.03	8580	0	2	588017977829818403	14190772+3510588
60	4	14:19:24.77	35:07:42.73	13.06	-0.01	8538	0	2	587736940371247301	14192476+3507427
61	1	14:27:34.68	11:19:50.06	10.45	-0.06	7993	2	1	588017704556888172	14273466+1119498
61	2	14:27:14.54	11:20:21.00	11.12	-0.05	8324	2	1	588017704556888080	14271453+1120212
61	3	14:27:22.36	11:16:17.32	12.78	-0.06	8162	0	2	587736478664556756	14272235+1116172
61	4	14:27:33.02	11:22:12.03	12.81	-0.06	7424	0	2	588017704556888164	14273302+1122118
62	1	14:28:16.36	25:50:55.61	9.33	-0.03	4497	24	1	587739720299577472	14281635+2550557
62	2	14:28:07.23	25:52:07.60	10.18	-0.03	4371	2	1	587739707410415672	14280724+2552077
62	3	14:28:13.47	25:56:50.76	10.72	-0.02	4021	2	1	587739707410415654	14281346+2556507
62	4	14:27:50.79	25:50:17.11	11.27	-0.03	4405	3	1	587739720299577369	14275077+2550172
63	1	14:58:46.22	-19:16:00.69	8.48	-0.02	3350	11	1	000000000000000000	14584622-1916006
63	2	14:57:21.72	-19:12:49.32	9.67	-0.02	3423	45	1	000000000000000000	14572172-1912491
63	3	14:58:55.06	-19:14:20.70	10.44	-0.02	3291	45	1	000000000000000000	14585504-1914206
63	4	14:58:50.11	-19:03:35.76	10.82	-0.03	3521	24	1	000000000000000000	14585010-1903356
64	1	15:35:57.01	43:29:35.42	9.62	-0.04	5659	47	1	587733411526606950	15355700+4329351
64	2	15:36:42.17	43:32:21.68	10.31	-0.04	5566	2	1	587733411526672449	15364216+4332217
64	3	15:36:27.08	43:31:07.59	10.53	-0.03	6038	2	1	587733411526672426	15362709+4331075
64	4	15:36:02.79	43:30:12.37	11.45	-0.04	5597	2	1	587733411526606951	15360279+4330122
64	5	15:36:35.19	43:25:32.24	12.30	-0.05	5768	0	2	587733411526672511	15363521+4325326
65	1	16:12:40.14	33:02:05.55	10.51	-0.06	9601	3	1	587736783607365679	16124014+3302054
65	2	16:12:41.33	33:02:15.64	11.19	-0.05	9446	0	1	587736783607365680	16124129+3302158
65	3	16:13:00.77	33:02:07.08	12.99	-0.04	9368	0	2	587736783607365887	16130077+3302069
65	4	16:12:56.70	33:03:05.93	13.26	-0.06	9410	0	2	587736783607365861	16125671+3303059
66	1	16:37:53.93	36:04:23.05	9.91	-0.06	9399	3	1	587733608555216981	16375395+3604233
66	2	16:37:59.89	35:59:43.85	11.18	-0.06	9618	2	1	587733603732422719	16375990+3559438
66	3	16:37:47.18	36:06:54.12	11.68	-0.05	9856	3	1	587733608555216924	16374718+3606543
66	4	16:37:48.44	36:03:39.14	12.71	-0.09	9609	0	2	587733603732357553	16374842+3603393
67	1	19:15:34.12	-54:37:36.11	9.48	-0.04	5546	45	1	000000000000000000	19153413-5437359
67	2	19:14:22.02	-54:33:56.18	10.31	-0.04	5134	30	1	000000000000000000	19142202-5433561
67	3	19:14:12.81	-54:34:26.91	10.97	-0.04	5252	22	1	000000000000000000	19141282-5434270
67	4	19:14:01.32	-54:35:15.60	12.25	-0.04	5549	45	2	000000000000000000	19140128-5435155
68	1	19:52:08.76	-30:49:30.98	9.47	-0.04	6012	11	1	000000000000000000	19520876-3049311
68	2	19:51:59.05	-30:48:57.17	10.07	-0.03	5805	45	1	000000000000000000	19515906-3048572
68	3	19:51:57.33	-30:51:23.99	10.64	-0.03	5233	45	1	000000000000000000	19515735-3051241
68	4	19:51:51.94	-30:48:30.38	11.07	-0.04	5976	45	1	000000000000000000	19515192-3048301
69	1	20:00:58.42	-47:04:12.85	10.02	-0.04	6355	18	1	000000000000000000	20005841-4704130
69	2	20:00:56.84	-47:05:03.87	10.40	-0.05	7070	54	1	000000000000000000	20005684-4705040
69	3	20:01:05.26	-47:03:33.97	11.80	-0.06	6792	45	2	000000000000000000	20010526-4703340
69	4	20:00:53.58	-47:05:42.51	11.96	-0.03	6815	44	2	000000000000000000	20005354-4705424
70	1	20:03:27.03	-55:56:49.81	8.01	-0.03	4433	26	1	000000000000000000	20032702-5556498
70	2	20:02:47.25	-56:05:25.10	8.82	-0.03	4391	76	1	000000000000000000	20024726-5605250
70	3	20:03:01.06	-55:56:52.88	9.97	-0.03	4388	33	1	000000000000000000	20030107-5556528
70	4	20:03:41.79	-55:54:55.68	10.95	-0.03	4590	19	1	000000000000000000	20034177-5554557
71	1	20:18:19.15	-70:51:31.77	7.77	-0.03	4009	16	1	000000000000000000	20181914-7051317
71	2	20:16:56.50	-70:46:05.67	8.37	-0.03	4554	30	1	000000000000000000	20165648-7046057
71	3	20:19:29.62	-70:51:35.56	9.29	-0.02	3928	22	1	000000000000000000	20192966-7051356
71	4	20:15:23.88	-70:32:15.87	10.50	-0.03	3479	30	1	000000000000000000	20152387-7032159
72	1	20:43:45.71	-26:33:00.99	10.45	-0.07	12221	92	1	000000000000000000	20434570-2633011
72	2	20:43:49.67	-26:35:32.19	11.76	-0.06	12131	45	2	000000000000000000	20434965-2635321
72	3	20:43:33.67	-26:35:10.11	12.15	-0.06	12589	45	2	000000000000000000	20433370-2635101
72	4	20:43:38.11	-26:34:17.42	12.66	-0.07	12631	0	2	000000000000000000	20433810-2634171
73	1	20:47:19.06	00:19:14.94	8.89	-0.02	4200	2	1	587731173842026987	20471908+0019150
73	2	20:47:24.29	00:18:02.99	9.65	-0.02	3790	2	1	587731173842027210	20472428+0018030
73	3	20:47:34.09	00:24:41.89	9.97	-0.03	3768	20	1	587731173842092228	20473408+0024420
73	4	20:47:07.24	00:25:48.66	10.65	-0.02	3663	2	1	587730847960596651	20470724+0025486
73	5	20:47:10.50	00:21:47.90	11.13	-0.03	3715	2	1	587731173842026895	20471048+0021479
73	6	20:47:20.35	00:29:02.36	11.35	-0.03	4228	2	1	587730847960596912	20472035+0029020
74	1	20:52:35.46	-05:42:40.06	9.85	-0.04	5968	2	1	587727214416953538	20523547-0542399
74	2	20:52:29.69	-05:44:45.97	10.22	-0.04	6128	2	1	587727214416953446	20522971-0544459
74	3	20:52:26.02	-05:46:19.86	12.06	-0.05	5995	4	2	587727214416953420	20522602-0546198
74	4	20:52:12.74	-05:47:53.63	12.25	-0.02	6060	4	2	587726878873486063	20521275-0547538

Table C2 – *continued* — Table of galaxy positions

GroupID	GalID	RA	Dec	K	k_K	v	$\text{err}(v)$	v	SDSS_ID	2MASS_ID
		(J2000)				[km s ⁻¹]		source		
75	1	21:08:32.01	-29:46:08.58	9.57	-0.04	5914	45	1	000000000000000000	21083199-2946083
75	2	21:07:59.93	-29:50:08.89	10.87	-0.04	5954	31	1	000000000000000000	21075991-2950089
75	3	21:08:58.28	-29:46:58.14	11.44	-0.04	5855	31	1	000000000000000000	21085826-2946582
75	4	21:08:10.63	-29:39:04.87	11.78	-0.03	5985	31	2	000000000000000000	21081059-2939049
76	1	21:16:55.29	-42:15:36.06	9.46	-0.04	5325	19	1	000000000000000000	21165529-4215361
76	2	21:16:46.19	-42:15:42.05	10.11	-0.04	5151	45	1	000000000000000000	21164619-4215421
76	3	21:17:27.92	-42:20:22.93	10.70	-0.04	5348	33	1	000000000000000000	21172789-4220231
76	4	21:16:47.80	-42:23:47.45	12.41	-0.04	5409	0	2	000000000000000000	21164779-4223471
77	1	22:03:30.92	12:38:12.38	9.83	-0.05	8041	7	1	587730774413213871	22033093+1238124
77	2	22:03:30.31	12:39:38.75	11.15	-0.05	7895	2	1	587730774413213915	22033031+1239384
77	3	22:03:22.58	12:38:57.53	12.09	-0.03	8184	0	2	587730774413214125	22032258+1238574
77	4	22:03:33.46	12:38:54.46	12.79	-0.04	8897	0	2	587730774413213877	22033345+1238544
78	1	22:36:27.96	-24:20:30.34	10.30	-0.06	10215	37	1	000000000000000000	22362797-2420306
78	2	22:36:20.35	-24:16:40.42	11.74	-0.06	10392	45	1	000000000000000000	22362036-2416406
78	3	22:36:25.77	-24:19:54.72	12.30	-0.07	10414	45	2	000000000000000000	22362578-2419546
78	4	22:36:23.15	-24:16:46.55	12.50	-0.08	10235	0	2	000000000000000000	22362315-2416466
79	1	22:55:20.45	-33:53:16.47	10.21	-0.05	8507	45	1	000000000000000000	22552046-3353166
79	2	22:55:22.38	-33:53:41.70	11.23	-0.06	8734	38	1	000000000000000000	22552239-3353416
79	3	22:55:18.62	-33:55:13.71	12.39	-0.06	8787	150	2	000000000000000000	22551861-3355136
79	4	22:55:27.79	-33:53:49.80	12.79	-0.07	8938	0	2	000000000000000000	22552777-3353496
80	1	22:57:57.52	26:09:00.01	9.25	-0.05	7375	21	1	758883828517699894	22575750+2609000
80	2	22:58:19.56	26:03:43.03	10.59	-0.05	7662	23	1	758883828517765263	22581956+2603431
80	3	22:57:51.71	26:09:43.75	11.72	-0.05	7587	0	1	758883828517699852	22575170+2609436
80	4	22:58:24.96	26:10:12.28	12.16	-0.04	7233	0	2	758883828517765149	22582499+2610119
80	5	22:57:56.56	26:06:39.86	12.24	-0.06	7654	0	2	758883828517765157	22575655+2606400
81	1	23:15:16.08	18:57:41.04	9.00	-0.03	5072	20	1	758883880592736344	23151609+1857409
81	2	23:15:03.46	18:58:24.24	10.04	-0.03	4772	10	1	758883828521304188	23150347+1858245
81	3	23:15:17.26	19:02:29.98	10.39	-0.03	4736	3	1	758883880592670819	23151728+1902299
81	4	23:15:33.06	19:02:53.24	11.11	-0.04	5173	34	1	758883880592736265	23153308+1902529
82	1	23:28:17.74	-67:49:16.92	9.82	-0.02	3903	40	1	000000000000000000	23281779-6749170
82	2	23:27:36.97	-67:48:55.66	10.27	-0.02	3905	45	1	000000000000000000	23273700-6748557
82	3	23:28:21.97	-67:45:36.91	11.37	-0.03	3882	45	1	000000000000000000	23282200-6745369
82	4	23:28:30.81	-67:45:40.73	11.49	-0.02	4290	45	1	000000000000000000	23283081-6745409
83	1	23:28:35.11	32:24:56.65	9.18	-0.03	5131	22	1	000000000000000000	23283508+3224565
83	2	23:28:10.77	32:28:22.36	10.78	-0.03	4544	36	1	000000000000000000	23281075+3228224
83	3	23:28:23.17	32:21:44.54	10.84	-0.03	4999	29	1	000000000000000000	23282316+3221445
83	4	23:28:31.60	32:25:19.68	11.37	-0.03	5277	26	1	000000000000000000	23283161+3225195
84	1	23:47:22.99	-02:18:02.42	10.07	-0.04	6932	22	1	000000000000000000	23472298-0218025
84	2	23:47:18.91	-02:18:48.60	10.71	-0.05	6327	30	1	000000000000000000	23471891-0218485
84	3	23:47:23.79	-02:21:04.55	11.03	-0.04	6003	26	1	000000000000000000	23472378-0221045
84	4	23:47:37.84	-02:19:00.03	11.56	-0.05	6817	45	1	000000000000000000	23473787-0218598
84	5	23:47:19.86	-02:16:50.78	12.72	-0.06	6664	0	0	000000000000000000	23471984-0216505
85	1	23:53:53.88	07:58:13.99	9.15	-0.03	5373	22	1	587743797290008717	23535389+0758138
85	2	23:53:26.79	07:52:32.36	9.52	-0.03	5106	7	1	587743797290008586	23532680+0752322
85	3	23:53:19.66	07:52:15.34	9.71	-0.04	5218	7	1	587743797289943215	23531967+0752152
85	4	23:53:32.15	08:07:05.27	10.66	-0.03	5154	58	1	587743960499159116	23533218+0807052
85	5	23:53:45.98	07:51:37.72	10.77	-0.04	5661	29	1	587743959962288248	23534595+0751377

Notes. Group ID, Galaxy ID, RA: Right Ascension, Dec: Declination, K_b : Galactic Extinction-corrected K -band apparent magnitude, k -corr: k -correction in the K -band computed from Chilingarian et al. (2010) as a function of redshift and colour $H-K$, v_r : radial velocity, err_{v_r} : error in radial velocity, v_r _source: catalogue from which the v_r and err_{v_r} were extracted, SDSS_ID: Object ID in the SDSS-DR7 database, 2MASS_ID: ID in the 2MASS database

References for redshift source:

- 1= main 2MRS (Huchra et al. 2012)
- 2= extra 2MRS (Huchra et al. 2012)
- 3= 2M++ redshift catalogue (Lavaux & Hudson 2011)
- 0= NED